Sedimentary Geology 501 (2026) 107124

Contents lists available at ScienceDirect

Sedimentary Geology

journal homepage: www.elsevier.com/locate/sedgeo

Skeletal assemblage fluctuations within persistent Mediterranean coral-reef framework during Cenozoic warming events☆

Luca Mariani [a], Giovanni Coletti [b,*], Alessandro Vescogni [a], Alberto Vimercati [b], Francesca R. Bosellini [a]

[a] Dipartimento di Scienze Chimiche e Geologiche, Università di Modena e Reggio Emilia, Via Giuseppe Campi 103, 41125, Modena, Italy
[b] Dipartimento di Scienze dell'Ambiente e della Terra, Università degli Studi di Milano-Bicocca, Piazza della Scienza 1, 20126, Milano, Italy

ARTICLE INFO

Editor: Dr. Michal Gradzinski

Keywords:
Carbonate factory
EECO
LOWE
MMCO
Benthic foraminifera
Calcareous algae

ABSTRACT

Coral reefs face severe threats from global warming and pollution, yet predicting their long-term response is hindered by the limited duration of ecological observations. This study investigates the geological record to examine the sedimentary and biotic composition of three Cenozoic reef systems developed during major warming events: the Early Eocene Climatic Optimum (EECO), the Late Oligocene Warming Event (LOWE), and the Middle Miocene Climatic Optimum (MMCO). We performed quantitative analysis of 247 thin sections from Monte Postale (NE Italy, EECO), Castro Limestone (SE Italy, LOWE), and Dağpazarı (S Türkiye, MMCO), focusing on shallow-water facies and organic buildups. Results show that while all intervals supported framework reefs with moderate-to-high coral diversity, the carbonate factory compositions varied significantly. The EECO reef system is characterized by abundant foraminifera and reduced coral contribution, reflecting a crisis in coral production likely driven by extreme temperatures. The LOWE reef system displays a peak in coral abundance, favored by less extreme temperatures, low nutrient levels, and optimal Mg/Ca ratio. The MMCO reef system shows a slight decline in corals compared to the Oligocene, with a concurrent increase in red algae and heterotrophs potentially linked to carbon cycle perturbations. These results are backed by data on the stratigraphic distribution of coral-dominated facies, an independent proxy of coral carbonate production. Overall, this highlights the resilience of the reef factory, which, as testified by the textural characteristics of the investigated limestones and by the persistence of the coral dominance in the buildups, maintains its overall structural integrity under diverse warming scenarios, being compromised only by extreme thermal anomalies or by a combined effect of multiple stressors.

1. Introduction

Modern coral reefs represent some of the most biodiverse and socio-economically significant ecosystems globally, yet they are increasingly vulnerable to the synergistic effects of anthropogenic stressors and climate change (Pandolfi et al., 2003; Sarkar and Ghosh, 2013; Hughes et al., 2017a; Eddy et al., 2021). Rising sea-surface temperatures, ocean acidification, and localized impacts, such as eutrophication and overfishing, threaten a near-total collapse of reef frameworks by the end of the century under high-emission scenarios (Hoegh-Guldberg et al., 2007; Hughes et al., 2017b; IPCC, 2022). Consequently, reef corals (i.e., zooxanthellate and mostly colonial tropical corals), the primary engineers of these ecosystems, face heightened extinction risks as they are among the carbonate producers most sensitive to thermal anomalies and associated bleaching events (Carpenter et al., 2008; Hughes et al., 2017a; Cheung et al., 2021).

While debate persists regarding specific extinction thresholds (e.g., Dietzel et al., 2021), the long-term viability of these systems hinges on two critical pillars: the maintenance of taxonomic biodiversity and the sustained capacity for carbonate production and accretion (Bosellini et al., 2025). Understanding the long-term trajectories of these features is essential for predicting the survival of the coral-reef ecosystem. However, the short-term nature (decades) of ecological observations limits our ability to forecast long-term (hundreds, thousands, or millions of years) responses to thermal stress. The geological archive, therefore, serves as the primary repository of observable data for contextualizing

☆ This article is part of a Special issue entitled: 'Carbonate' published in Sedimentary Geology.

* Corresponding author.
E-mail address: giovanni.coletti@unimib.it (G. Coletti).

https://doi.org/10.1016/j.sedgeo.2026.107124
Received 25 February 2026; Received in revised form 12 May 2026; Accepted 28 May 2026
Available online 1 June 2026

current ecosystem shifts against past periods of elevated global temperatures (Pandolfi and Kiessling, 2014; Tierney et al., 2020).

Previous studies have investigated the ecological consequences of past reef crises to provide insights on the fate of contemporary reef systems (Bridge et al., 2022). Others have performed comparative analysis between coral diversity and reef development in the past, yielding contradictory results and revealing complex relationships between biodiversity and reef development. While some data suggest a positive correlation between these factors over long timescales (e.g., Kiessling, 2005; Bosellini et al., 2021), other points to a decoupling of diversity and framework growth (e.g., Kiessling and Baron-Szabo, 2004; Johnson et al., 2008; Zamagni et al., 2012; Perrin and Bosellini, 2012, 2013; Bosellini et al., 2022; Bosellini et al., 2025). This decoupling underlines how high biodiversity does not necessarily imply the presence of large reef frameworks and vice-versa, even if optimal conditions undoubtedly correspond to a system's ability to maintain both high coral diversity and robust reef-building capacity. This suggests that reef development and coral diversity may be governed by distinct drivers (e.g., SST, nutrients, CO_2 levels); specifically, reef accretion appears more sensitive to climate warming than taxonomic richness, implying that warm climates may inherently constrain reef growth regardless of warming rates (Coletti et al., 2022; Bosellini et al., 2025).

Coral morphology also represented a focus of the research aimed at understanding the future of coral reefs, investigating the morphological traits of reef corals in both modern (Madin et al., 2016a) and fossil records (e.g., Raja et al., 2022; Bridge et al., 2022; Dimitrijević et al., 2023; Bosellini et al., 2026). Modern reefs have shown that specific traits determine coral function, their influence on the environment, and their responses to environmental and anthropogenic stressors (Madin et al., 2016b; Denis et al., 2017; Fontoura et al., 2020). Trait-based paleontological approach has been attempted particularly for deciphering long-term ecosystem behavior during major thermal perturbations (Pandolfi and Kiessling, 2014; Dee et al., 2019; Tierney et al., 2020). Although fossil morphological responses occasionally deviate from modern climate-driven trends (Bosellini et al., 2026), other instances demonstrate remarkable consistency between deep-time and contemporary trait shifts (e.g., Dimitrijević et al., 2023).

Consequently, while the decoupling of biodiversity from reef-building potential and the limitations of trait-based paleontological approaches suggest that the geological record is not a direct one-to-one forecast for modern reefs, it remains an irreplaceable archive for identifying ecological tipping points, recovery trajectories, and the adaptive capacity of corals under thermal stress.

In this work, we address future trajectories of the reef environment by focusing not only on reef corals and the frameworks they develop, but also on the other biogenic sedimentary components associated with these ecosystems, i.e., the carbonate factory. The most significant carbonate producers associated with coral reefs are red calcareous algae (RCA), green calcareous algae (GCA), large benthic foraminifera (LBF), small benthic foraminifera (SBF), and encrusting benthic foraminifera (EBF), along with various heterotrophic calcifiers such as mollusks, bryozoans, echinoderms, serpulids and crustaceans (Pomar, 2001; Pomar and Hallock, 2008; Reijmer, 2021). While coral calcification may decrease under thermal stress, total reef carbonate production reflects a complex interplay of processes, and some components may even respond positively to rising temperatures (Bialik et al., 2023), further highlighting the inadequacy of predicting the future of coral reefs based exclusively on coral-specific data. Given their high preservation potential, biogenic deposits of marine invertebrate carbonate producers provide a unique perspective on long-term environmental trajectories. While individual occurrences may lack the high-resolution detail of modern ecological datasets, their spatial extent and abundance offer a trove of useful information. Unfortunately, the lack of quantitative data on carbonate deposits, especially skeletal assemblages, hinders integration and cross-comparison, preventing a rigorous assessment of hypotheses regarding their temporal evolution (Kiessling et al., 1999; Coletti et al., 2022; Bialik et al., 2023). Nevertheless, abundance-based approaches to the study of skeletal components have been increasingly applied to microfacies and stratigraphic investigations (e.g., Brandano et al., 2009; Guido et al., 2016, 2021; Mariani et al., 2024). This approach excels at capturing large-scale environmental shifts as it backs hypotheses with hard data. Furthermore, by focusing on higher taxonomic levels, it mitigates the inherent challenges of species-level classifications.

In light of these considerations, the main goal of this work is to trace the changes in the skeletal composition of three well studied Cenozoic reef-bearing carbonate systems of the Mediterranean corresponding to three distinct warm periods: the Early Eocene Climatic Optimum (EECO), the Late Oligocene Warming Event (LOWE) and the Middle Miocene Climatic Optimum (MMCO).

The EECO (53.3–49.1 Ma; Ypresian) represented a prolonged interval of elevated temperatures, with global mean surface temperatures of about ~10–15 °C above modern levels (Burke et al., 2018; Scotese et al., 2021; Inglis et al., 2020; Westerhold et al., 2020), accompanied by high atmospheric pCO_2 levels (Rae et al., 2021), and marked by a considerable decline in coral reef volume (Kiessling and Baron-Szabo, 2004).

The LOWE (26.5–24 Ma; Chattian; average global temperatures ~3–5 °C above modern levels; Zachos et al., 2001; Zhang et al., 2013; O'Brien et al., 2020; Westerhold et al., 2020) was a warm interval characterizing the latest part of the Paleogene. During the LOWE luxuriant coral reefs developed worldwide (Johnson et al., 2008; Mihaljević et al., 2017; Pomar et al., 2017; Coletti et al., 2022), featuring, on average, moderately-to-highly diverse scleractinian associations (Budd, 2000; López-Pérez, 2005; Bosellini and Perrin, 2008).

The MMCO (17–15 Ma; late Burdigalian–Langhian; average global temperatures ~3–8 °C above modern levels; You et al., 2009; Goldner et al., 2014; Burke et al., 2018; Westerhold et al., 2020; Steinthorsdottir et al., 2021) temporarily interrupted the late Cenozoic cooling trend. During this period, the coral reef belt attained its maximum latitudinal extent of the Miocene (Perrin and Kiessling, 2012; Perrin and Bosellini, 2012; Wiedl et al., 2013), although corals were often replaced by red calcareous algae as the main tropical carbonate producers (Halfar and Mutti, 2005).

The selected three key-coral reef settings that developed within these warm phases are the following:

1) For the EECO, the upper Ypresian Monte Postale deposits (MP; NE Italy), characterized by small coral buildups, with calcareous algae and encrusting foraminifera contributing to the bioconstruction (Vescogni et al., 2016);
2) For the LOWE, the upper Oligocene reef complex of the Castro Limestone (CL; S Italy), characterized by a flourishing reef coral faunal association (Bosellini and Russo, 1992; Bosellini and Perrin, 1994; Bosellini, 2006; Pomar et al., 2014; Bosellini et al., 2021);
3) For the MMCO, the coral reef system of the Dağpazarı carbonate platform (DCP; S Türkiye), characterized by abundant contribution of coralline algae (Vescogni et al., 2014).

Despite their different ages and paleogeographic settings, these coral reefs share several important features: (1) they developed in shallow-water, purely carbonate environments; (2) they formed wave-resistant frameworks; and (3) they exhibit moderate to high coral diversity. Based on these similarities, we aim to compare their skeletal assemblages in order to assess whether significant changes occurred in their composition and/or whether certain characteristics persisted through time. A quantitative analysis of the skeletal assemblages in these reef systems should allow for the recognition of both shared and divergent trends. Such insights will improve our knowledge about Cenozoic ecological dynamics providing clear lens for interpreting modern changes in reef ecosystems and strengthening our predictive models.

2. Geological setting of the studied sites

2.1. Monte Postale coralgal buildups (MP)

2.1.1. Geological setting

The Monte Postale is located in the Lessini Mountains, in the northeast of the Italian Peninsula (Fig. 1A). This area belongs to the Southern Alps, a structural unit corresponding to the northernmost corner of the Adriatic Plate (Schmid et al., 2004; Márton et al., 2011; Carminati et al., 2012; Handy et al., 2015). The tectonic evolution of this area, accompanied by significant volcanic activity, led in the early Eocene to the uplift of several blocks, that reached the photic zone forming a carbonate platform known as the Lessini Shelf (Fig. 1B) (Doglioni and Bosellini, 1987; Bosellini, 1989; Luciani, 1989; Bassi et al., 2008). These Eocene shallow-water deposits, commonly referred to as the "Calcari Nummulitici" (Nummulitic Limestones) (Bosellini et al., 1967; Carraro et al., 1969; De Zanche et al., 1977; Sarti, 1980; Ungaro, 2001), include the Monte Postale coralgal buildups.

2.1.2. Depositional model and age

The Monte Postale coralgal buildups crop out as a discontinuous alignment of massive to weakly stratified limestones, with a limited lateral extent of about 200 m and a maximum thickness of 13.7 m. The stratigraphic architecture of these limestones and their facies distribution were described in detail by Vescogni et al. (2016), who identified three distinct facies associations (Fig. 2A):

a) Fore reef: stratified deposits including a coralgal rudstone facies, located in a more proximal position and derived from erosion of the overlying coralgal rim, and an *Alveolina–Nummulites* packstone facies occurring in a relatively more distal position.
b) Coralgal rim: a massive coralgal margin forming the central "backbone" of the buildups. The bioconstructed portions of this structure consist of a coralgal boundstone facies (in situ scleractinian coral colonies and solenoporacean algae) associated to a polygenic bindstone facies (in situ encrusting foraminifera, scleractinian corals, peyssonneliacean, solenoporacean, and coralline red algae). These facies are interspersed with coralgal rudstone debris, derived from erosion of the preceding facies, and *Alveolina* grainstone deposits.
c) Lagoon: the lagoonal facies association displays a well-stratified succession of laminated and non-laminated wackestones deposits. In proximity to the coralgal rim, these deposits may be interbedded with a graded *Alveolina* grainstone facies, interpreted as the result of resedimentation of *Alveolina* grainstones from the coralgal rim.

The age of the Monte Postale coralgal buildups was determined based on analyses of *Alveolina* and calcareous nannofossil assemblages. These two datasets respectively allowed the identification of the SBZ 11 (Serra-Kiel et al., 1998) and CNE 5 (Agnini et al., 2014) biozones, establishing a late Ypresian age, spanning from approximately 50.5 to 48.96 Ma (Vescogni et al., 2016).

2.2. Castro Limestone coral reef (CL)

2.2.1. Geological setting

The Castro Limestone Formation crops out in the Salento Peninsula, at the southeastern corner of the Italian Peninsula (Fig. 1A). This region belongs to the Apulia Platform (Fig. 1D), one of the main structural domains of the Adriatic Plate. Since the Late Cretaceous the Salento Peninsula has been occupied by an isolated, shallow-water carbonate platform. Sedimentation was primarily influenced by moderate-amplitude sea-level fluctuations, leading to the formation of several, relatively thin, vertically stacked sequences mainly concentrated in the distal portion of the plateau. Lying upon an Upper Cretaceous basement, these units range in age from the middle Eocene to the Early Pleistocene and include clinostratified bioclastic successions and coral reef systems (Fig. 1E) (Bosellini et al., 1999; Ricchetti and Ciaranfi, 2013; Milli et al., 2024). Among the latter, the Chattian Castro Limestone represents the most spectacular example, with well-preserved back reef, reef front and slope facies.

2.2.2. Depositional model and age

The Castro Limestone coral reef is a large structure, extending for a total length of 28 km, a maximum width of 3 km, and a thickness ranging from 5 to over 100 m (Bosellini and Russo, 1992). As one of the best-preserved Oligocene coral reefs in the Mediterranean, the Castro Limestone has received considerable attention over time, with studies focusing on various aspects of the depositional system, including its age, depositional geometries, characterization and reef-building role of the coral assemblage (Rossi, 1969; Bosellini and Russo, 1992; Parente, 1994; Bosellini and Perrin, 1994; Bosellini, 2006; Pomar et al., 2014; Bosellini et al., 2021).

Bosellini et al. (2021), tracing a palaeobathymetric transect of the reef system, recognized the succession of five main palaeoenvironments and related facies (Fig. 2B):

a) Distal slope: represented by clinostratified beds containing large amounts of scleractinian colonies, either fragmented or preserved whole, forming floatstone to rudstone accumulations. Some coral colonies in life position may also occur. The matrix surrounding the corals consists of bioclastic grainstones and packstones with relatively abundant planktic foraminifera.
b) Proximal slope: similarly to the distal slope, these deposits consist of thick clinobeds with abundant coral fragments, irregularly scattered or concentrated in floatstone to rudstone deposits and few in situ colonies. The matrix is also composed of bioclastic grainstones and packstones, but with a lower proportion of planktic foraminifera compared to the distal slope.
c) Reef front: it is the main bioconstructed margin of the reef system, consisting of a massive framework formed by in situ scleractinian colonies and a minor contribution from coralline red algae. Coral rubble deposits are also widespread, together with bioclastic calcarenite and calcirudite accumulations showing variable textures.
d) Outer back reef: massive to weakly stratified, poorly cemented deposits made of coarse bioclastic packstones and grainstones. Corals are represented by few, large colonies in life position.
e) Inner back reef: massive to weakly stratified deposits composed of coarse bioclastic packstones and grainstones. Compared to the outer back reef, the coral fauna here consists of a greater number colonies, generally large, mostly in growth position, occurring either scattered or forming small clusters.

Based on the occurrence of *Miogypsinoides* sp., the Castro Limestone Formation has been attributed to the SBZ23 of Cahuzac and Poignant (1997), indicating an age corresponding to the middle-upper Chattian (see discussion in Bosellini et al., 2021).

2.3. Dağpazarı coral reef (DCP)

2.3.1. Geological setting

The Dağpazarı coral reef complex is situated within the Mut Basin, one of the Neogene intramontane basins that border the present-day southern coast of Türkiye (Fig. 1A). It is located in the central Tauride Mountains (Fig. 1F), along the southern edge of the Anatolian Plateau. The general compressional tectonic regime affecting this area since the Paleozoic has resulted in a complex intramontane landscape, which served as a substrate for the deposition of upper Oligocene to Lower Miocene continental deposits. These were followed by shallow-marine carbonates assigned to the Mut Formation (upper Burdigalian–Serravallian) (Fig. 1G), which includes the Dağpazarı coral reef. The overall structure of the Mut Formation displays a thickness up to 1100 m and consists of a succession of broad, stacked shallow-marine

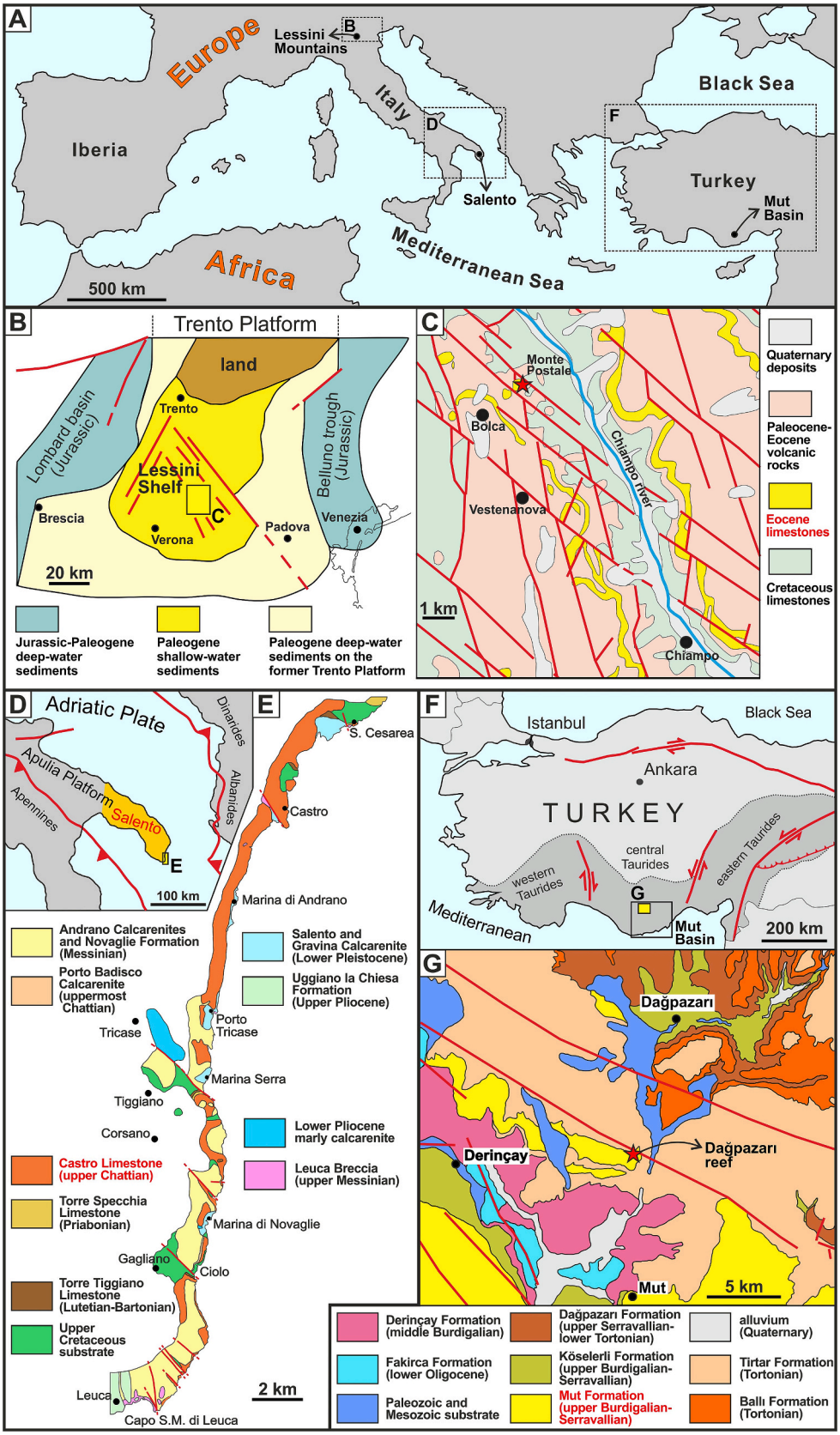

Fig. 1. A) Schematic map of the Mediterranean highlighting the locations of the areas associated with the three reef systems considered. B) Palaeogeographic reconstruction of the Paleogene Lessini Shelf (modified from Bosellini, 1989). C) Geological map of the Monte Postale area (modified from Muscio and Tintori, 2005). D) Map of the south-eastern portion of the Italian Peninsula showing the main tectonic elements (modified from Milli et al., 2024). E) Geological map of the south-eastern coastal strip of the Salento Peninsula (modified from Bosellini et al., 1999). F) Schematic map of Türkiye showing the main tectonic elements and the location of the Mut Basin (modified from Bassant et al., 2005). G) Geological map of the Dağpazarı area (modified from Ilgar et al., 2019).

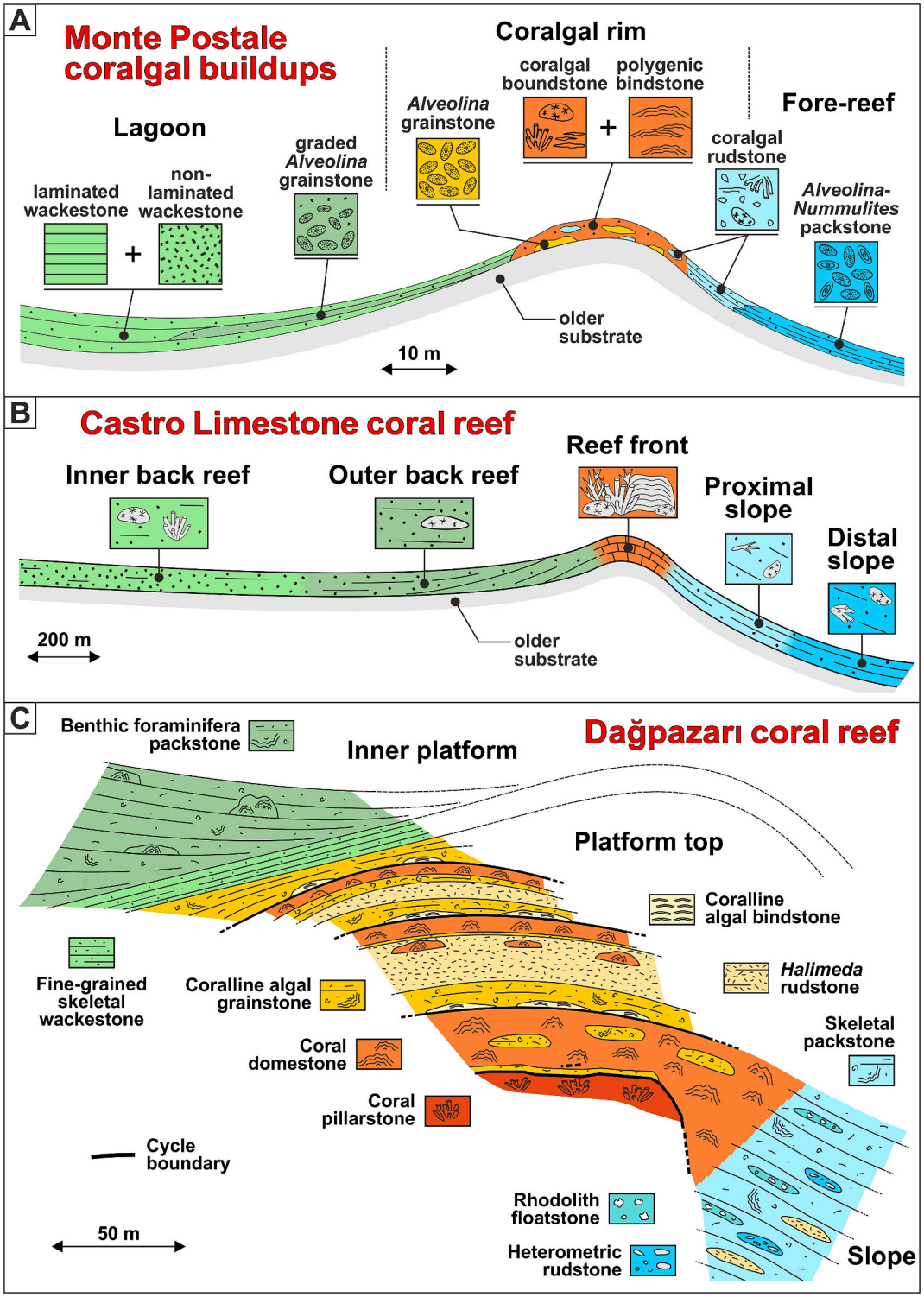

Fig. 2. Palaeobathymetric profiles showing the distribution of facies/facies associations of: A) the Monte Postale coralgal buildups (modified from Vescogni et al., 2016); B) the Castro Limestone coral reef (modified from Bosellini et al., 2021); C) the Dağpazarı coral reef (modified from Vescogni et al., 2014).

carbonate sequences, representing successive stages of marine transgression (Bassant et al., 2005; Bassant and Gürbüz, 2005; Janson et al., 2010; Ilgar et al., 2019).

2.3.2. Depositional model and age

The Dağpazarı coral reef measures about 1000 m in length and roughly 400 m in width, with a maximum thickness of about 72 m. Based on stratigraphic, sedimentological, and facies analyses, Vescogni et al. (2014) developed a depositional model comprising three facies associations (Fig. 2C):

a) Slope: this relatively distal portion of the reef complex includes several distinct facies: floatstone accumulations composed of rhodoliths formed by coralline red algae, encrusting foraminifera, and serpulids; *Halimeda* rudstone deposits dominated by chaotically arranged green algal plates; heterometric rudstones interpreted as

more distal and associated with storm events. All these facies are enclosed within a bioclastic skeletal packstone.

b) Platform top: this facies association includes several vertically stacked facies, whose arrangement reflects the succession of different depositional cycles. Within these cycles, the bioconstructed portions of the reef system are mainly represented by a coral domestone facies, characterized by massive scleractinian colonies in life position, and a coral pillarstone facies, containing in situ branching and phaceloid colonies. A subordinate reef-building role is also played by a coralline algal bindstone facies, composed of coralline red algae and encrusting foraminifera. On the platform top, bioclastic sediments are mainly represented by grainstones particularly rich in coralline algal fragments, and *Halimeda* deposits similar to those of the slope facies association.

c) Inner platform: two distinct facies characterize this landward portion of the reef system, represented by a fine-grained skeletal wackestone, followed by a benthic foraminifera packstone interspersed by small, bioconstructed coral patches.

The age of the Dağpazarı coral reef was determined by combining nannoplankton biostratigraphic analyses from the underlying carbonate succession, which indicate an age no older than the early Langhian (Bassant et al., 2005), with Sr isotope data from oysters sampled from the considered sections, which yielded an age between 16 and 15.6 Ma (latest Burdigalian to early Langhian) (Vescogni et al., 2014). Accordingly, the age of the reef system was assigned to the early Langhian (see discussion in Vescogni et al., 2014).

Table 1
Comparison of the original microfacies from the three studied sites with the Wilson's (1975) SFZ. For MP, highly altered samples, such as the ones from the microfacies "recrystallized limestones" and "diagenetic breccias", were omitted from the quantitative dataset, also because they do not belong to a specific Wilson's facies.

SFZ (Wilson, 1975)	MP (Vescogni et al., 2016)	CL (Bosellini et al., 2021)	DCP (Vescogni et al., 2014)
Foreslope (4)	- *Alveolina* and nummulitid limestones	- Distal reef slope - Proximal reef slope	- Skeletal packstone - Heterometric rudstone - Rhodolith floatstone - *Halimeda* rudstone
Organic Buildup (5)	- Massive coralgal limestone - *Alveolina* grainstone	- Reef front	- Coralline algal bindstone - Coralline algal grainstone - Coral domestone - Coral pillarstone
Winnowed Edge Sands (6)	- Graded *Alveolina* grainstone	- Outer back reef	
Open Circulation Shelf Lagoon (7)		- Inner back reef	- Benthic foraminifera packstone - Fine-grained skeletal wackestone
Restricted Lagoon (8)	- Non-laminated wackestone		

3. Materials and methods

We quantitatively analysed the skeletal assemblages of the selected Cenozoic reef systems focusing on photic-zone facies representing bioconstructed coral margins or genetically related environments, such as fore-reef slopes and lagoons. A total of 247 thin sections (MP: 88; CL: 63; DCP: 96), housed at the University of Modena and Reggio Emilia, were examined. These samples were mainly derived from previously published studies (Vescogni et al., 2014, 2016; Bosellini et al., 2021) and were collected from reef-related sediments along stratigraphic sections or through random sampling within the deposits. Thin sections originally prepared specifically for coral taxonomic analyses were intentionally excluded in order to avoid any bias toward primary framebuilders (i.e., reef corals). To capture both the overall variability (as determined through ordination analysis) and the average composition of the carbonate factories, a substantial number of thin sections were analysed, with over 50,000 data points per site for a total of approximately 180,000 points.

To standardize the analysis among the three sites, we grouped the original microfacies (see Vescogni et al., 2014, 2016 and Bosellini et al., 2021 for the original microfacies identifications and descriptions) into the Standard Facies Zones of Wilson (1975), focusing on Foreslope (SFZ 4), Organic Buildup (SFZ 5), Winnowed Edge Sands (SFZ 6), Open Circulation Shelf Lagoon (SFZ 7), and Restricted Lagoon (SFZ 8) (Fig. 2; Table 1).

Quantitative analysis of the skeletal assemblages was performed using the point-counting technique (Flügel, 2010; Coletti et al., 2021). A minimum of 500 points per thin section were counted (on randomly acquired photomicrographs of the sections) using a 250 μm grid (see Supplementary Materials 1). Given the wide stratigraphic range of the study, spanning from the Eocene to the Miocene, textural and skeletal components were organized into 25 functional categories. Textural components are subdivided into: macroporosity, authigenic fraction, detrital fraction, sparite, micrite, unidentifiable bioclastic sand, skeletal grains, and non-skeletal grains. Skeletal components were grouped based on their ecological behavior rather than on purely taxonomic affinity. This approach allowed for the grouping of taxa with shared environmental responses, including light, nutrient availability, temperature, sedimentation, and feeding strategies. For example, *Orbitolites* and *Sorites* were grouped together into a single 'porcelaneous LBF' category. Skeletal components include the following categories: unidentified bioclasts, corals, red calcareous algae (RCA; comprising both geniculate and non-geniculate RCA, and corallinacean, peyssonneliacean and solenoporacean algae), green calcareous algae (GCA; of the order dasycladales, including *Halimeda* and *Acetabularia*), hyaline LBF (comprising amphisteginids/asterigerinids, orthophragmines, lepidocyclinids, miogypsinids, unidentified lepidocyclinids/miogypsinids, *Nummulites*, *Operculina*, *Heterostegina*, *Spiroclypeus*, unidentified nummulitids, and other large symbiont-bearing hyaline taxa), porcelaneous LBF (comprising *Orbitolites*, soritids, alveolinids, *Borelis*, *Dendritina*, *Archaias*, other large symbiont-bearing miliolids), agglutinated LBF (large symbiont bearing textulariids), hyaline small benthic foraminifera (hyaline SBF; comprising small rotaliids), porcelaneous SBF (comprising small miliolids, *Austrotrillina*), agglutinated SBF (small textulariids), hyaline encrusting benthic foraminifera (hyaline EBF; including encrusting acervulinids and planorbulinoidids such as *Acervulina*, *Miniacina*, *Sphaerogypsina*, and *Fabiania*), porcelaneous EBF (nubeculariids), agglutinated EBF (such as *Haddonia*), planktic foraminifera (PLK), mollusks (MOL, comprising bivalves, gastropods and tusk shells), echinoderms (ECH), sessile heterotrophs (comprising barnacles, serpulids, encrusting serpulids, bryozoans), and mobile arthropods (MA, ostracods and decapods). After collecting raw data from the thin sections, we calculated the relative abundance of every component and consequently quantified the average abundance per Wilsons's facies of each component in each site. To further evaluate environmental gradients, paleobathymetric parameters, specifically the H/P ratio (hyaline vs. porcelaneous benthic foraminifera; Coletti et al., 2021; Mariani et al., 2024, 2025) was calculated across the dataset. Furthermore, as the primary objective of this study is to characterize the variability within bioconstructed facies, the analysis focused extensively on Wilson's SFZ 5 (Organic buildup). This targeted approach facilitated a high-resolution comparison of the similarities and differences within the skeletal assemblages. Ordination analysis, using Bray-Curtis similarity index (Bray and Curtis, 1957), was applied to the quantitative microfacies dataset to minimize a priori biases and assess the known variability of the systems (Bialik et al., 2021). This technique spatially organizes samples based on

their similarities in a multivariate space, thereby highlighting complex relationships and potential environmental gradients across the studied sites (Gauch and Whittaker, 1972; Syms, 2008). The resulting data clusters, comprising all points from each site, offer a comprehensive 2D representation of the variability of the analysed carbonate systems within the multivariate space. Two different types of ordination were used: Non-metric Multi-Dimensional Scaling (NMDS) and Detrended Correspondence Analysis (DCA). As an indirect gradient analysis, NMDS produces an ordination by replacing the original distance between data with ranks, thereby avoiding issues associated with absolute distance (Kruskal, 1964). DCA is a derivative of the correspondence analysis method (Hill, 1979). Correspondence analysis determines the relative position of elements by maximizing correspondence rather than variance between variables and data points; however, it is susceptible to an "arch effect," which is adjusted in the detrended correspondence analysis, resulting in a better portrayal of the relationships between variables. Both NMDS and DCA analyses were performed using R software, using an updated version of the code published by Bialik et al. (2021). The Bray-Curtis index (Bray and Curtis, 1957) was employed for the analysis of the dataset.

4. Results

The quantitative results derived from the point-counting analysis across the three study sites and their respective Standard Facies Zones (SFZs) are summarized in Tables 2 and 3, and in Fig. 3. The comprehensive raw datasets are provided in Supplementary Material 1. The following sections first detail the general sedimentological and compositional trends across all facies, followed by a specific comparative analysis of SFZ 5 (i.e., the Organic Buildup), in alignment with the primary objective of comparing bioconstructed facies across the three sites.

4.1. Overall results

4.1.1. Textural components

Quantitative analysis reveals distinct sedimentological and textural signatures across the different SFZs (Table 2; Fig. 3), but broadly similar patterns emerge when specifically comparing the SFZ 5 "Organic Buildup" across all sites.

At MP, the relative abundance of skeletal components increases progressively from the foreslope (SFZ 4: 24.7%) through the organic buildup (SFZ 5: 53.2%) to the winnowed edge sands (SFZ 6: 65.2%), before decreasing significantly in the restricted lagoon (SFZ 8: 11.8%). In contrast, CL is characterized by a more relevant skeletal fraction across all facies (SFZ 4: 62.3%; SFZ 6: 49.9%; SFZ 7: 51.1%), peaking at 82.2% within the organic buildup SFZ 5 (the highest value recorded in this study across all sites). In DCP skeletal grains largely dominate the organic buildup (SFZ 5: 73.2%) and are very relevant in the foreslope (SFZ 4: 51.6%) and the shelf lagoon (SFZ 7: 44.3%).

Unidentified bioclasts are mainly represented by poorly preserved large grains and are minor constituents of most facies, generally accounting for <5% of the total grains and consistently much lower than their identified counterparts. The only exception are the MP winnowed-edge sands (SFZ 6), where unidentified bioclasts reach 6.8% of the limestone (compared to 58.4% for identified skeletal grains). Overall, the average skeletal content (identified + unidentified bioclasts) is the highest at CL (61.4%), closely followed by DCP (56.4%), and lower in MP (38.7%).

Non-skeletal grains are rare at all sites, peaking at 1.8% and 1.3% in MP SFZ 4 and SFZ 6, respectively. The detrital terrigenous fraction is negligible, with a maximum value of 0.8% recorded at MP SFZ 4. Authigenic minerals are largely absent, except for rare occurrences of glauconite in the CL foreslope (SFZ 4: 0.2%). Macroporosity is likewise limited, with maximum values observed in CL SFZ 6 (3.1%), CL SFZ 7 (2.3%), and DCP SFZ 7 (2.6%).

Sparite is a common constituent across all facies and sites. At MP, sparite peaks in SFZ 6 (16.2%) and remains relatively stable in other zones (SFZ 4: 11.1%; SFZ 5: 9.8%; SFZ 8: 8.9%). At CL, sparite abundances are comparable across the foreslope and lagoonal facies (SFZ 4: 9.7%; SFZ 6: 7.3%; SFZ 7: 8.7%), with the lowest concentration in the organic buildup (SFZ 5: 5.8%). At DCP, sparite content fluctuates from 12.4% and 11.8% in SFZ 4 and SFZ 7 to 6.7% in SFZ 5. Mean sparite values are consistent across the study areas: MP (11.5%), DCP (10.3%), and CL (7.9%).

Matrix composition is largely dominated by unidentifiable, sand-sized, bioclastic material, which consistently outbalance micrite across all sites and consists of unrecognizable fragments of larger skeletal grains. The sole exception is found in the MP restricted lagoon (SFZ 8), where micrite reaches 36.7%. However, even here, it remains secondary to sand-sized matrix (42.3%). The sand-sized fraction is particularly dominant in the MP foreslope (SFZ 4: 57.9%) and remains ubiquitous in other facies, reaching its minimum in CL's organic buildup (SFZ 5: 10.8%). On average, MP exhibits a higher sand content (36.6%) than DCP (27.1%) and CL (25.2%). Micrite ranges from rare to common; it remains below 5% in all MP facies except for SFZ 8. In the other sites, micrite peaks in the CL shelf lagoon (SFZ 7: 6.3%) and DCP foreslope (SFZ 4: 7.6%), respectively. Overall, the highest average micrite concentration is recorded at MP (11.7%), compared to DCP (4.7%) and CL (4.1%).

4.1.2. Carbonate producers

Corals constitute one of the most prominent skeletal groups across the study areas (Table 3). At MP, they reach a maximum abundance of 48.7% within the organic buildup (SFZ 5), while concentrations are markedly lower in the remaining facies (SFZ 4: 10.3%; SFZ 6: 4.5%; SFZ 8: 13.5%) (Table 3, Fig. 4). CL exhibits a higher coral abundance, peaking in the organic buildup (SFZ 5: 84.0%), followed by the foreslope (SFZ 4: 64.2%), shelf lagoon (SFZ 7: 55.0%), and winnowed edge sands (SFZ 6: 26.0%). Notably, coral abundance in CL exceeds that of the corresponding zones of the other two sites (Fig. 4). CL also exhibits the highest average coral abundance (57.3%), which is more than double that of MP (19.3%) and DCP (22.1%). At DCP, the highest coral concentration is also found in SFZ 5 (52.2%), with values decreasing in SFZ

Table 2
Textural components abundance in the three sites. SFZ 4: foreslope; SFZ 5: organic buildup; SFZ 6 winnowed edge sands; SFZ 7: shelf lagoon open circulation; SFZ 8: shelf lagoon restricted circulation.

	Monte Postale (MP)					Castro Limestone (CL)					Dağpazarı Carbonate Platform (DCP)				
	SFZ 4	SFZ 5	SFZ 6	SFZ 7	SFZ 8	SFZ 4	SFZ 5	SFZ 6	SFZ 7	SFZ 8	SFZ 4	SFZ 5	SFZ 6	SFZ 7	SFZ 8
Macroporosity	0,7	1,2	0,59	\	0,3	0,2	0,1	3,1	2,3	\	0,7	0,5	\	2,6	\
Authigenic minerals	0	0	0	\	0	0,2	0	0	0	\	0	0,01	\	0	\
Sparite	11,1	9,8	16,2	\	8,9	9,7	5,8	7,3	8,7	\	12,4	6,7		11,8	\
Terrigenous fraction	0,2	0,02	0	\	0,02	0	0	0,01	0,01	\	0,01	0,01	\	0	
Micrite	3,7	4,2	2,1	\	36,7	3,9	1,1	5,1	6,3	\	7,6	2,9	\	3,6	\
Unidentifiable bioclastic sand	57,9	31,5	14,6	\	42,3	23,6	10,8	34,7	31,6	\	27,3	16,6	\	37,6	
Non skeletal grains	1,8	0,1	1,3	\	0	0,1	0	0	0	\	0,4	0,2	\	0,1	\
Skeletal components	24,7	53,2	65,2	\	11,8	62,3	82,2	49,9	51,1	\	51,6	73,2	\	44,3	

Table 3
Identified skeletal components abundance in the three sites. SFZ 4: foreslope; SFZ 5: organic buildup; SFZ 6 winnowed edge sands; SFZ 7: shelf lagoon open circulation; SFZ 8: shelf lagoon restricted circulation.

	Monte Postale (MP)					Castro Limestone (CL)					Dağpazarı Carbonate Platform (DCP)				
	SFZ 4	SFZ 5	SFZ 6	SFZ 7	SFZ 8	SFZ 4	SFZ 5	SFZ 6	SFZ 7	SFZ 8	SFZ 4	SFZ 5	SFZ 6	SFZ 7	SFZ 8
Corals	10,34	48,73	4,52	\	13,52	64,24	83,99	26,01	55,00	\	13,28	52,16	\	0,85	
RCA	1,72	9,49	0,00	\	4,29	11,91	5,03	31,85	15,99	\	25,31	28,28	\	53,34	
GCA	0,00	0,76	0,33	\	0,00	0,03	0,00	0,00	0,00	\	29,29	1,08	\	0,00	
LBF hyaline	18,97	3,28	4,36	\	0,69	9,29	4,59	17,93	8,59	\	2,31	2,33	\	7,62	
LBF porcelaneous	31,90	13,91	81,03	\	9,85	0,47	0,42	0,53	0,63	\	0,42	0,82	\	0,80	
LBF agglutinated	0,00	0,07	0,00	\	1,04	0,00	0,00	0,00	0,00	\	0,00	0,00	\	0,00	
SBF hyaline	9,48	3,00	1,64	\	28,01	2,84	0,88	4,79	4,01	\	4,14	1,95	\	8,12	
SBF porcelanoeus	15,52	3,31	3,73	\	21,92	1,77	0,81	4,00	1,89	\	1,30	1,07	\	1,91	
SBF agglutinated	0,00	0,51	0,55	\	1,65	0,55	0,47	1,31	0,47	\	0,73	0,20	\	0,65	
EBF hyaline	6,90	10,09	0,77	\	0,99	1,90	1,31	2,61	1,88	\	3,07	3,97	\	5,24	
EBF porcelanous	0,00	0,11	0,44	\	0,00	0,05	0,02	0,61	0,19	\	0,43	0,64	\	0,21	
EBF agglutinated	0,00	0,34	0,00	\	0,14	0,17	0,22	0,18	0,00	\	0,54	0,38	\	0,33	
PLK	0,00	0,01	0,00	\	0,00	0,24	0,00	0,04	0,00	\	0,47	0,02	\	0,31	
Mollusks	3,45	3,03	1,10	\	5,20	1,48	0,58	2,33	0,66	\	8,00	2,56	\	6,22	
Sessile heterotrophs	0,00	0,57	0,00	\	0,07	1,35	0,28	0,42	0,95	\	3,56	1,43	\	1,48	
Echinoderms	0,00	2,12	1,43	\	1,13	3,05	1,30	6,57	9,04	\	5,35	2,37	\	10,72	
Mobile arthropods	1,72	0,68	0,11	\	11,49	0,66	0,10	0,82	0,71	\	1,80	0,76	\	2,21	

4 (13.3%) and becoming negligible in SFZ 7 (0.9%; Fig. 4).

Red calcareous algae (RCA) represent another major skeletal component (Table 3). At MP, RCA peak in SFZ 5 (9.5%) but decrease consistently in the other facies (SFZ 4: 1.7%; SFZ 8: 4.3%). RCA abundance is generally higher in CL, reaching 31.9% in SFZ 6, 16% in SFZ 7, 11.9% in SFZ 4, and a minimum of 5.0% in SFZ 5. DCP displays the highest RCA abundance, with values always above 25.0%, peaking at 53.3% in the open lagoon settings (SFZ 7). DCP also exhibits the highest average RCA abundance (35.6%), followed by CL (16.2%) and MP (3.9%). In contrast to RCA, green calcareous algae (GCA) are minor constituents across all sites (Table 3). They are only relevant in the DCP foreslope (SFZ 4), where they are abundant (29.3%). Overall, calcareous algae (RCA + GCA) reach their maximum cumulative abundance in DCP, followed by CL and MP (Table 2, Fig. 3).

Large benthic foraminifera (LBF) are also a major skeletal component in all sites (Table 3). Hyaline LBF peak in the MP foreslope (SFZ 4: 19.0%) and in the winnowed edge sands of CL (SFZ 6: 17.9%), while at DCP they display lower abundances reaching only 7.6% (SFZ 7). The site-wide average abundance of hyaline LBF is the highest at CL (10.1%), followed by MP (6.8%) and DCP (4.1%). Porcelaneous LBF are remarkably more relevant than their hyaline counterparts at MP, reaching 81.0% in SFZ 6, 31.9% in SFZ 4, and 13.9% in SFZ 5. Conversely, they remain below 1.0% across all facies in CL and DCP. Consequently, the average abundance of porcelaneous LBF values is high at MP (34.2%) but negligible at DCP (0.7%) and CL (0.5%). Agglutinated LBF are restricted to MP, occurring in trace amounts with a maximum abundance of 1.0% in SFZ 8.

Small benthic foraminifera (SBF) follow similar a similar pattern of distribution. Hyaline SBF are most abundant at MP, specifically in SFZ 8 (28.0%) and SFZ 4 (9.5%), while values at CL and DCP generally below 5.0% (with the exception of DCP SFZ 7: 8.1%). MP exhibits the highest average abundance of hyaline SBF (10.5%), which is more than double that of DCP (4.7%) and triple that of CL (3.1%). Similarly to their hyaline counterparts, porcelaneous SBF peak at MP, in the restricted settings (SFZ 8: 21.9%) and in the foreslope (SFZ 4: 15.5%). CL and DCP record consistently lower values (< 4.0%). Similarly to porcelaneous LBF, MP also exhibits the highest average abundance of porcelaneous SBF (11.1%) (CL: 2.1%; DCP: 1.4%). Agglutinated SBF are generally rare, peaking in the restricted settings of MP (SFZ 8: 1.7%), with all other facies recording lower values (≤ 1.3%).

Encrusting benthic foraminifera (EBF) with hyaline test peak at MP in SFZ 5 (10.1%) and SFZ 4 (6.9%). Their presence diminishes sharply in the other MP facies. They are very rare at CL and rare in DCP, peaking in SF7 (5.2%) (Table 3). On average, hyaline EBF are more abundant in MP (4.7%), followed by DCP (4.1%) and CL (1.9%). Porcelaneous and agglutinated EBF are always rare (< 0.7%).

Planktic foraminifera (PLK) are virtually absent across all sites and facies, with a maximum abundance of only 0.5% in the DCP foreslope (SFZ 4).

Mollusks are ubiquitous, with peak abundances in the DCP foreslope (SFZ 4: 8.0%) and shelf lagoon (SFZ 7: 6.2%) (Table 3). In MP, they reach 5.2% (SFZ 8). In CL values are lower, peaking at 2.3% (SFZ 6). DCP shows the highest average mollusk abundance (5.6%), followed by MP (3.2%) and CL (1.3%). Sessile heterotrophs are rare on average (less than 1.5% in MP and CL), but comparatively more relevant in DCP (SFZ 4: 3.6%). Echinoid concentrations are significant in the lagoonal settings of DCP (SFZ 7: 10.7%) and CL (SFZ 7: 9.0%), in the foreslope of DCP (SFZ 4: 5.4%) and in the winnowed edge sands of CL (SFZ 6: 6.6%), whereas they are less abundant in MP (peaking at 2.1% in SFZ 5). Free-living crustaceans (e.g., ostracods) are most frequent in the restricted lagoon of MP (SFZ 8: 11.5%) and never exceed 2.2% in all other facies and sites.

4.2. Ratio of hyaline to porcelaneous foraminifera

The H/P ratio, calculated as the ratio between hyaline large and small benthic foraminifera (LBF + SBF) relative to their porcelaneous counterparts, exhibits significant variations across the different facies and sites (Table 4). The highest values are generally recorded in foreslope facies (SFZ 4) and particularly in the foreslope of CL (5.4) which displays higher values than those of DCP (3.8) and significantly higher than those of MP (0.6). CL displays the highest values of H/P also in the organic buildup facies (4.4 compared to the 2.3 of DCP and 0.4 of MP). Within lagoonal settings the H/P parameters is 5.8 in DCP, 5.0 in CL, and 0.9 in MP. Winnowed edge sands occur only in CL and MP and once again CL displays higher values (5.0 against the 0.1 of MP).

4.3. Organic buildup (SFZ 5)

At MP, the total abundance of skeletal components is lower than the other sites (around 1/2 of the rock compared to an average of 3/4 in the other sites; Fig. 3A). However, when skeletal grains are excluded from the analysis, the abundance of the remaining components reveals clear textural similarities across the three organic buildups (Fig. 3B). The matrix composition is remarkably consistent: unidentifiable sand-sized fragments constitute the primary component, supplemented by broadly equivalent amounts of micrite across all sites (Table 2). Detrital and authigenic fractions, as well as non-skeletal grains, are virtually

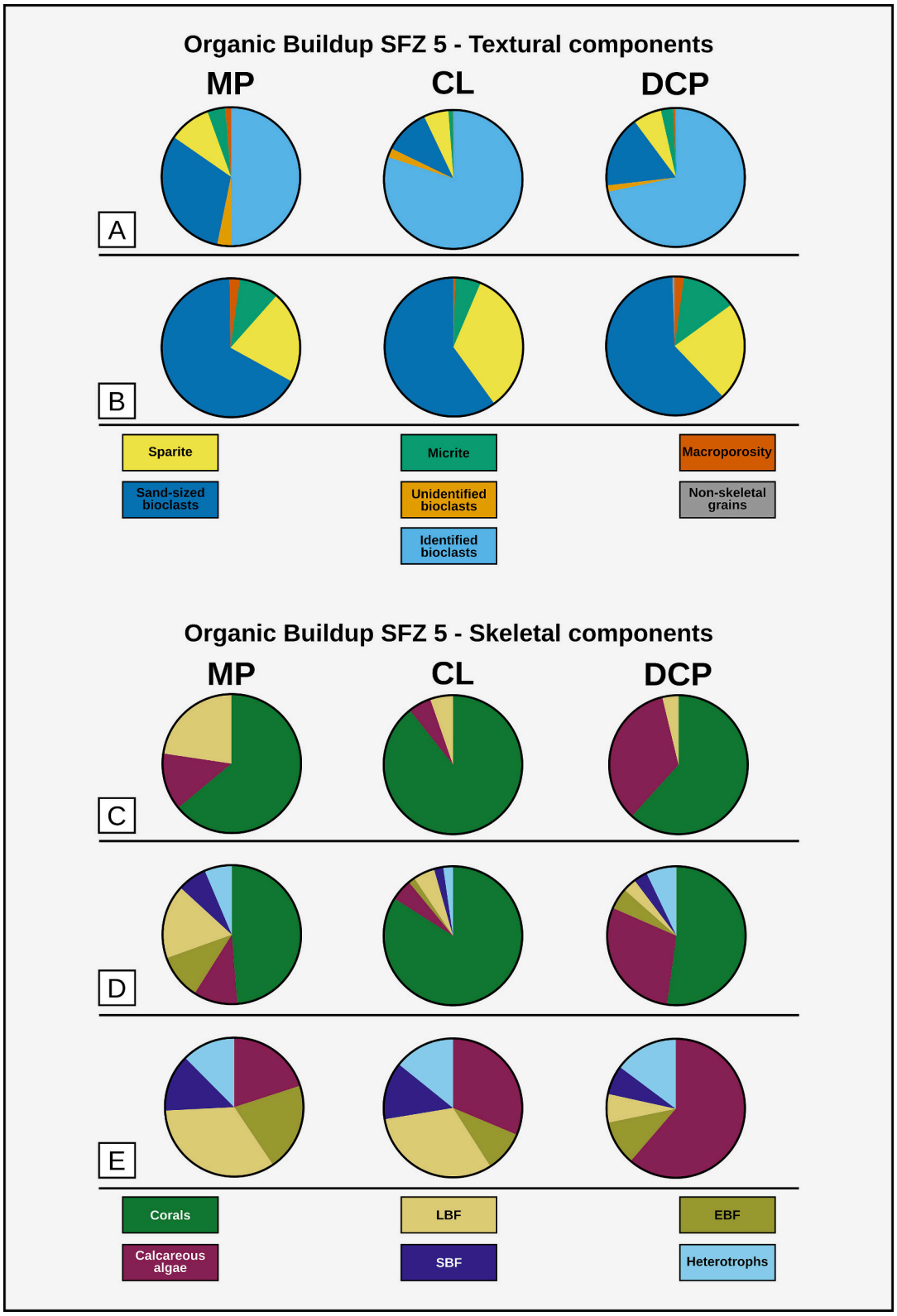

Fig. 3. Comparative compositional analysis of the Organic Buildup (SFZ 5) across the three study sites: Monte Postale (MP), Castro Limestone (CL), and the Dağpazarı carbonate platform (DCP). A) Total sedimentary constituents: pie plots illustrating the distribution of textural components alongside total identified and unidentified skeletal fractions. B) Normalized textural composition: distribution of non-skeletal textural components calculated by excluding the total skeletal fraction to highlight background sedimentological similarities. C) Primary carbonate producers: comparison of the three dominant skeletal components, i.e., corals, calcareous algae (RCA + GCA), and large benthic foraminifera (LBF). D) Comprehensive skeletal assemblage: detailed breakdown of all identified skeletal components, illustrating the full taxonomic diversity of the bioconstructed facies. E) Secondary biotic components: pie plots representing the skeletal assemblage normalized without the coral fraction to emphasize the relative proportion of the other producers.

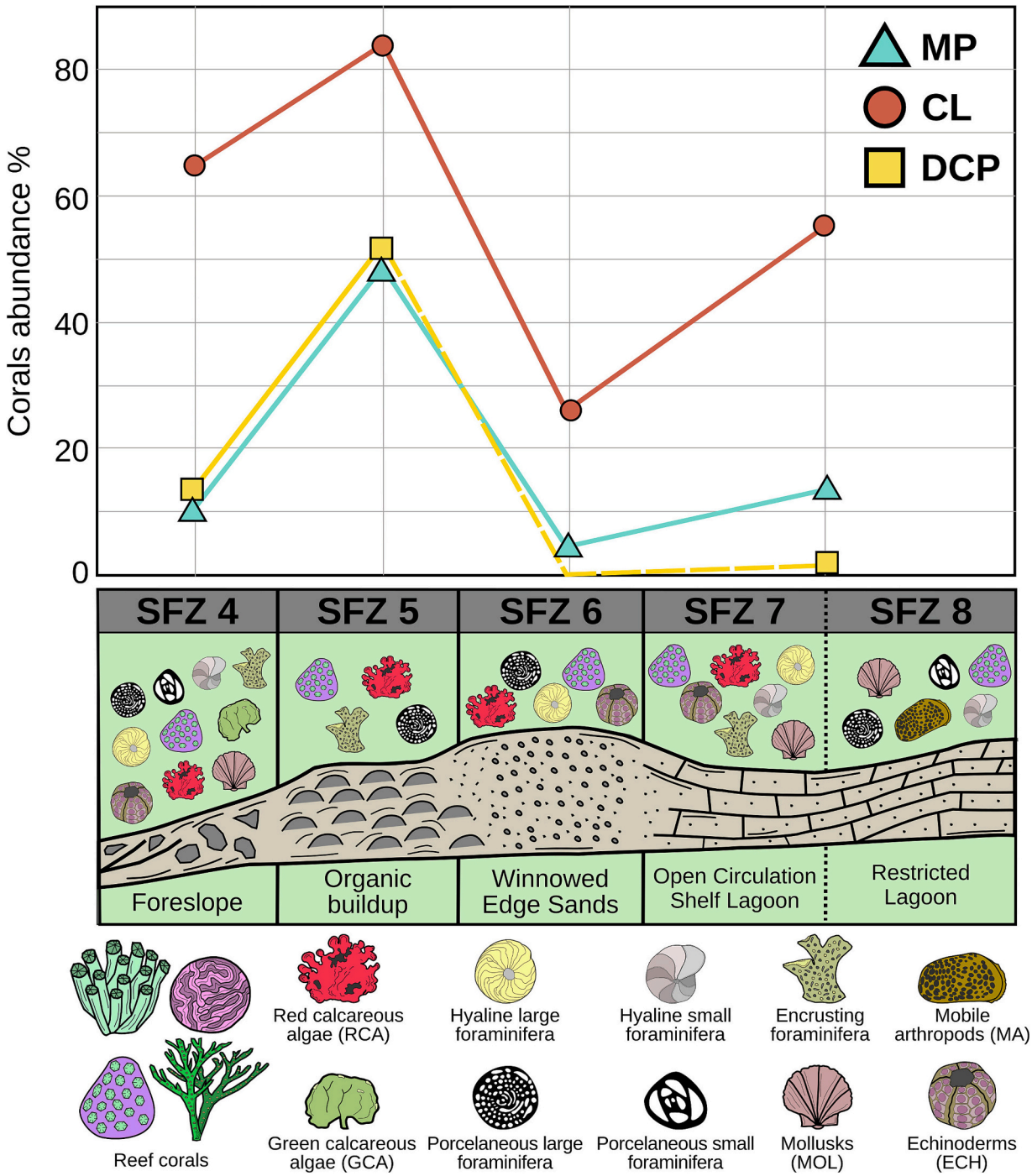

Fig. 4. Comparative coral distribution and facies model. Top: Line graph illustrating the relative abundance (%) of corals across the identified Standard Facies Zones (SFZ 4 to SFZ 8) for the three study sites: Monte Postale (MP; teal line), Castro Limestone (CL; red line), and Dağpazarı carbonate platform (DCP; yellow line). Note the consistent peak in coral dominance within the organic buildup (SFZ 5) across all sites and the significantly higher coral values maintained at Castro Limestone. For the purposes of this comparative analysis across the three study sites, SFZ 7 and SFZ 8 were grouped together due to their shared lagoonal characteristics and depositional significance. Bottom: Schematic depositional model representing the spatial distribution of skeletal assemblages and associated SFZs. Symbols indicate the characteristic biotic components >5% within the different facies. Modified from Wilson's (1975) and Mattern (2022). SFZ 4: foreslpe; SFZ 5: organic buildup; SFZ 6: winnowed edge sands; SFZ 7: shelf lagoon open circulation; SFZ 8: lagoon restricted circulation.

Table 4
H/P (hyaline/porcelaneous benthic foraminiferal ratio) calculated within the various SFZ across the three studied sites.

	Monte Postale (MP)					Castro Limestone (CL)					Dağpazarı Carbonate Platform (DCP)				
	SFZ4	SFZ5	SFZ6	SFZ7	SFZ8	SFZ4	SFZ5	SFZ6	SFZ 7	SFZ8	SFZ4	SFZ5	SFZ6	SFZ7	SFZ8
H/P	0,6	0,4	0,1	\	0,3	5,4	4,4	5,0	5,0	\	3,8	2,3	\	5,8	\

absent. Macroporosity remains scarce and slightly more pronounced at MP (2.4%) and DCP (2.3%) than in CL (0.6%). Sparite is a significant constituent in all buildup facies, with values ranging from a maximum of 33.6% at CL to 22.8% at DCP and 21.3% at MP (Fig. 3). Bioclasts preservation in thin sections is broadly uniform; notably, unidentified bioclasts represent less than 3.5% of all components across all sites.

Regarding the skeletal assemblages, corals represent the dominant carbonate producers of the organic buildups at all three sites, though their relative dominance varies (Figs. 3C, D, E, 4; Table 3). Corals exert a much more prominent role in the skeletal framework of CL (84.0%) than in MP (48.7%) or DCP (52.2%). In contrast, RCA reach their highest relevance in DCP (28.3%) (MP: 9.5%, CL: 5.0%; Fig. 3C-E). GCA remain a rare component across all sites, though they are marginally more frequent at DCP (1.1%).

Hyaline LBF occur in comparable proportions across the three sites, consistently representing less than 5% of the assemblage (MP: 3.3%; CL: 4.6%; DCP: 2.3%; Table 3). A major divergence is marked by the porcelaneous LBF, which are nearly absent at CL and DCP but relevant at MP (13.9%), where they constitute the second most abundant skeletal group. Agglutinated LBF are negligible throughout; consequently, total LBF abundance exhibits a sharp decrease from the Eocene (MP: 17.3%) to the Oligocene (CL: 5%) and the Miocene (DCP: 3.2%) (Fig. 3C-E).

SBF are mainly represented by hyaline and porcelaneous taxa and they are generally uncommon, reaching their highest abundance at MP (6.8%) and never exceeding 4.0% at the other localities. A distinct trend is observed for hyaline EBF, which are notably more relevant at MP (10.1%) than at CL (1.3%) or DCP (4.0%) (Fig. 3C-E; Table 3). Porcelaneous and agglutinated EBF, along with PLK, are negligible in the examined build-ups (Table 3).

Heterotrophic carbonate producers are generally more abundant at MP and DCP than at CL, with the cumulative contribution of mollusks, sessile heterotrophs, echinoids, and free-living crustaceans reaching 6.4% at MP and 7.1% at DCP and only 2.3% at CL (Fig. 3C-E; Table 3).

4.4. Ordination analysis

The resulting plots, incorporating data from all facies across the studied sites, provide an overview of the known variability of each carbonate system within the multivariate space, expressed as the area of the data clusters including all samples from a certain site (Fig. 5). In the DCA the first two axes, DCA1 and DCA2, capture the bulk of the variability in the biotic composition of the carbonate factory. The vectors representing the most relevant buildup builders (corals, RCA, and EBF) mostly point toward the lower-left corner, forming high angles relative to the vectors of many heterotrophic carbonate producers. The vector for LBF, another major carbonate producer in these systems, points toward the upper-left, in the opposite direction to the serpulid (SERP) vector. The samples form CL, MP and DCP form distinct clusters (each symbol representing a sample) with varying degrees of overlap. The CL cluster (red circles) is characterized by a strong association with the corals vector, reflecting the high relative coral abundances recorded at the site, particularly in SFZ 5 and SFZ 4. In the MP cluster (blue triangles), samples variability is primarily driven by the LBF and SBF vectors, corresponding to the high percentages of porcelaneous LBF, and SBF within the site. The DCP cluster (yellow squares) is mainly defined by RCA, GCA, mollusks, echinoderms, bryozoan and serpulids, and in particular by the high abundance of RCA (in all the facies) and of GCA (in SFZ 4).

The NMDS plot (Fig. 5) provides a non-linear representation of the similarities among the carbonate factories of the three study sites. Carbonate producer vectors show a similar distribution to the DCA plot. The main buildup builders are more closely grouped, and the LBF vector still points in the opposite direction of the SERP vector. While the sites exhibit more overlap in the NMDS space than into the DCA, the ordination clearly identifies the same drivers of the variability in each reef system: CL (red circles) is centrally located but pulled strongly toward the lower-center by the corals vector, confirming that coral abundance is the defining feature of the CL samples across multiple facies; MP (blue triangles) shows the widest scatter (and thus variability), occupying most of the left and upper-left quadrants and is characterized by the LBF and SBF vectors, illustrating the dominance of foraminiferal assemblages at this Eocene site; DCP (yellow triangles) is positioned on the right side of the plot, and is primarily defined by its association of RCA, GCA, BRY, and SERP. The area of overlap between the three clusters contains vectors representing echinoderms and mollusks, suggesting that these heterotrophic groups are common elements across all three systems.

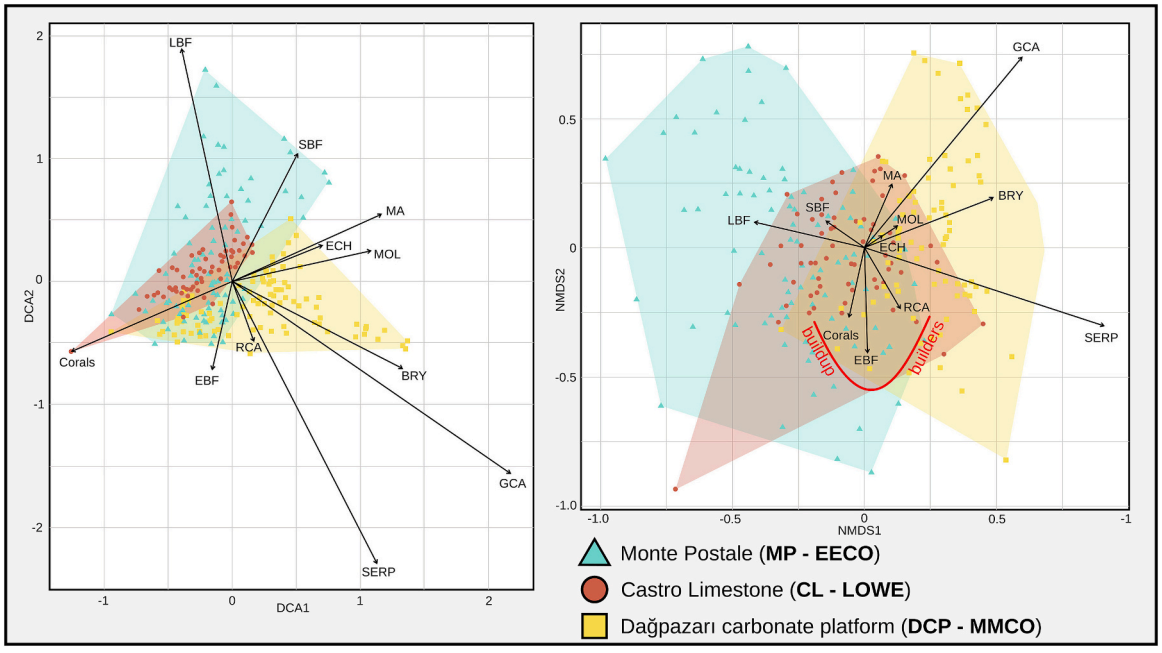

Fig. 5. Ordination analysis depicting the overall variability of the examined, reef-bearing, carbonate systems. Each cluster correspond to all samples from a given site. The extension of the clusters showcase in 2D the known variability of the system in the multivariate space.

5. Discussion

The analysed carbonate systems developed during various warm phases over a time span of approximately 34 million years, and their biotic composition was undoubtedly shaped by long-term evolutionary processes. Nevertheless, they formed within comparable depositional settings, namely, pure carbonate environments unaffected by siliciclastic input, as corroborated also by our data on the terrigenous fraction (Table 2). The overall similarity among these carbonate factories is also reflected in both textural and compositional evidence. The vast majority of the analysed facies consist of ~50% skeletal grains, ~30% of sand-sized comminuted bioclasts, and ~ 10% of sparite, along with other minor components (Table 2). The primary exceptions to this general pattern are represented by the fore-slope and restricted lagoon facies of the MP site (Table 2). The textural characteristics of the organic buildup facies are also remarkably consistent, with only the MP site displaying fewer than two-thirds skeletal grains (Table 2; Fig. 3). Indeed, while MP shows a slightly lower abundance of skeletal grains, the relative proportions of the remaining components are broadly similar (Fig. 3). The carbonate factories are all largely dominated by photozoan carbonate producers, specifically corals, calcareous algae, and symbiont-bearing foraminifera. Organic buildup facies are consistently dominated by corals, which account for at least ~50% of the identified skeletal assemblage (Table 3). Although the H/P ratio of the foraminiferal assemblage was originally designed for area-counting techniques (i.e., counting all foraminifera in a section; Mariani et al., 2024), and is thus likely to be less accurate when applied to point-counting data (where large individuals are over-represented), the results still suggest that the analysed facies of the CL and DCP systems developed at comparable water depths. In contrast, the preserved portion of the MP system likely represents a shallower setting. Due to this, MP is the only site among the three studied ones to feature a restricted lagoon; predictably, this is also the only facies characterized by a relatively high abundance of micrite and ostracods.

Overall, these data support a reasonable degree of similarity between the three sites, which is reflected by the considerable overlap among the three site-specific clusters in the ordination analysis (Fig. 5). This similarity justifies a more in-depth comparison of the skeletal assemblage of the analysed carbonate systems.

5.1. Comparative assessment of the analysed skeletal assemblage

While corals represent a major component across all sites, peaking in abundance within the organic buildup facies (Table 3; Fig. 4), the remainder of the skeletal assemblage highlights significant differences in the composition of the carbonate factories among the three systems. These biotic variations assist in framing the evolution of the reef ecosystem throughout Cenozoic warming events.

In the lower Eocene site, foraminifera and especially porcelaneous LBF, are strikingly more abundant than in the other sites (Table 3; Fig. 3). This is clearly depicted in the ordination analysis, where the MP cluster stretches further than the other ones along the direction of the LBF and SBF vectors (Fig. 5), indicating that the observed variability of the MP system is strongly controlled by the abundance of these two types of producers. The MP system likely developed in a very shallow and potentially restricted environment as indicated by the low H/P ratio (Mariani et al., 2024). An hypothesis that is in agreement with previous analysis (Vescogni et al., 2016). Consequently, lagoonal facies, where foraminiferal contribution is often significant, are strongly expressed. However, the difference compared to the other sites is so pronounced and widespread (occurring across all facies, including the organic buildup; Table 3) that it must underlie a fundamental difference in the carbonate factory architecture. In the geological record, LBF carbonate production appears resilient to warming events, with LBF dominated facies peaking in abundance during warm spells, while other groups decline (Scheibner and Speijer, 2008; Coletti et al., 2022; Ali et al., 2025). Data from modern environments indicate that LBF biodiversity is positively coupled with temperature (Beavington-Penney and Racey, 2004) and that these organisms can calcify across a much wider temperature range than more complex carbonate producers, such as corals (Marshall and Clode, 2004; Crabbe, 2008; Titelboim et al., 2019). Indeed, although relatively complex, LBF remain unicellular organisms. Thus, despite certain groups clearly pursuing a K-strategy compared to other foraminifera (Hottinger, 1982), their life cycles are inherently more flexible than those of multicellular organisms. Alveolinids, the most prominent group of porcelaneous LBF at the MP site, bloomed right after the PETM (e.g., Benedetti et al., 2024; Ali et al., 2025), and reached peak diversity during the warm early Eocene (Benedetti and Papazzoni, 2022), highlighting a remarkable adaptability to warm intervals. The overall decline in the skeletal contribution of LBF from the EECO (MP), through the LOWE (CL), and finally to the MMCO (DCP) (Table 2; Fig. 5), can therefore be interpreted as a result of the long-term cooling trend of the Cenozoic (Westerhold et al., 2020; Judd et al., 2024), combined with the progressive northward movement of the Mediterranean area (Dercourt et al., 2000). Encrusting benthic foraminifera, which have typically acted as secondary framework builders in reefs since the Jurassic (Granier, 2024), are also quite common in Eocene carbonate systems (Plaziat and Perrin, 1992; Coletti et al., 2022). Unsurprisingly, their abundance peaks in the organic buildup facies of the MP site (Table 3), further highlighting how the early Eocene hothouse was indeed favorable for foraminiferal carbonate production.

If the lower Eocene site is defined by foraminifera, the upper Oligocene site by corals (see below), the Middle Miocene site can be defined by calcareous algae and in particular by RCA. Coralline algae are usually the second most relevant buildup builders in modern tropical reefs and rank among the most common carbonate producers worldwide (Bialik et al., 2023). Compared to corals, RCA can adapt to and thrive in a much wider range of environmental conditions, including nutrient-rich settings (e.g., Halfar et al., 2006), high-latitude regions (e.g., Teichert, 2014; Pyko et al., 2025), and high-energy environments otherwise unfavorable for reef-building corals (e.g., Ladd et al., 1950; Rankey and Garza-Pérez, 2012). RCA are also significant carbonate producers across a much wider latitudinal range than GCA, even in shallow-water settings (Brandano et al., 2019, and references therein). While the adaptability of modern RCA is undeniable, their abundance in fossil deposits suggests a more complex pattern. RCA are relatively rare in Eocene deposits but fairly common in Paleocene, Oligocene, and Miocene strata (Pomar et al., 2017; Sarkar et al., 2022; Coletti et al., 2022, 2025), with a global peak in RCA-dominated facies recorded during the Middle Miocene (Halfar and Mutti, 2005). RCA biodiversity increased throughout most of the Cenozoic, reaching a remarkable peak during the Miocene (Aguirre et al., 2000). Furthermore, during the Miocene, the turnover from lower Paleogene and Cretaceous assemblages dominated by Sporolithales to more modern assemblages dominated by Hapalidiales and Corallinales was essentially completed (Aguirre et al., 2000). Consistently, the abundance of RCA across the three examined sites can be attributed to the combined effects of temperature, nutrient availability, and evolutionary trends. During the early Eocene, temperatures were likely excessive, resulting in limited carbonate production by RCA. During the late Oligocene, conditions were significantly more favorable; however, competition for available substrate with corals may have acted as a limiting factor. This improvement in ecological conditions for RCA can be observed in shallow marine carbonate factories where the competition from corals was less significant, such as those related to seagrasses. Indeed, during the Oligocene, the contribution of RCA to the seagrass factory (at least in the Mediterranean) increased significantly in comparison to the Eocene (Brandano et al., 2019). During the Middle Miocene, the increase in nutrient availability associated with the Monterey Event might have hindered coral fitness (Föllmi et al., 2005; Halfar and Mutti, 2005; Brandano et al., 2017). Conversely, the by-then fully diversified modern orders of RCA (Corallinales and Hapalidiales) were able to better deal

with the increased nutrient levels, much as they do today, leading to an increase of RCA contribution to carbonate production. Similarly to RCA, *Halimeda* (the most common green calcareous alga recorded in this study) exhibits greater flexibility than corals regarding nutrient availability (Teichberg et al., 2013; Reolid et al., 2024). This flexibility may explain its higher abundance within the DCP site.

Heterotrophic carbonate producers typically prevail whenever light is not the most readily available or abundant form of energy in the environment (Westphal et al., 2010; Michel et al., 2011; Bialik et al., 2023). Accordingly, their relatively high abundance at DCP may reflect the Mediterranean region's movement toward higher latitudes (relative to the Eocene and Oligocene) and the increased nutrient availability associated with the Monterey Event.

5.2. The role of corals and their relevance in Oligocene reefs

A detailed discussion of the role of corals across the three investigated warm intervals requires a clear distinction between EECO, LOWE, and MMCO. While the former represents a prolonged (~ 4 Ma) 'hothouse', the latter two were shorter (~2 Ma) and less extreme events within an overall 'coolhouse' climate state (You et al., 2009; Zachos et al., 2001; Goldner et al., 2014; Burke et al., 2018; O'Brien et al., 2020; Westerhold et al., 2020; Steinthorsdottir et al., 2021). Some reconstructions (e.g., Westerhold et al., 2020) suggest that the LOWE exhibited lower temperatures compared to the MMCO. Furthermore, while the LOWE was not associated with major carbon cycle perturbations, the MMCO occurred in tandem with the Monterey Event (Föllmi et al., 2005; Westerhold et al., 2020). Finally, while the MMCO happened during a period strongly influenced by an already established Antarctic ice sheet (Steinthorsdottir et al., 2021), the LOWE was the first relevant warm interval after the first major glacial event of the Cenozoic (Oi1, Westerhold et al., 2020). Consistently, our data indicate a major reduction in coral carbonate production during the EECO, with corals representing only 1/4 of the total limestone of the organic build-up (Tables 2, 3) (i.e., ~50% of the identified skeletal grains which in turn correspond to ~50% of the whole rock). This crisis in coral production is consistent with stratigraphic data indicating a low abundance of coral-dominated facies in the lower and middle Eocene in Central Asia (Coletti et al., 2022), in the Mediterranean (Zamagni et al., 2012; Pomar et al., 2017), and in South America (Aguilera et al., 2020). While this crisis did not correspond to a global decline in coral biodiversity (López-Pérez, 2005; Zamagni et al., 2012; Benedetti et al., 2024; Bosellini et al., 2025), the reduced carbonate production evidenced by microfacies and stratigraphic data clearly indicates that the EECO significantly challenged coral-reefs (Fig. 6).

The thermal anomaly of the MMCO was shorter and less severe; nonetheless, it was likely associated with an increase in nutrient availability that was detrimental to corals. The distribution of coral-dominated facies in the geological record is more controversial (or less consistent) for the MMCO compared to the EECO, with different studies yielding contrasting results regarding their abundance. Halfar and Mutti (2005) report an increase in RCA dominance and a global decline in coral reefs. López-Pérez (2005) notes a scarcity of data regarding Middle Miocene coral reefs in the eastern Pacific. Esteban (1996) reports a slight Langhian decline in reefs along the Atlantic coast of Europe, followed by a more widespread decline in the Mediterranean during the Serravallian. Perrin and Bosellini (2012) indicate that a decline in Mediterranean coral reefs only occurred during the late Serravallian (and thus after the MMCO). Furthermore, no significant decline in coral reefs abundance was reported during the Middle Miocene in the Caribbean (Johnson et al., 2008). Reef coral biodiversity was also not clearly impacted by the MMCO neither in the Caribbean nor in the Mediterranean region

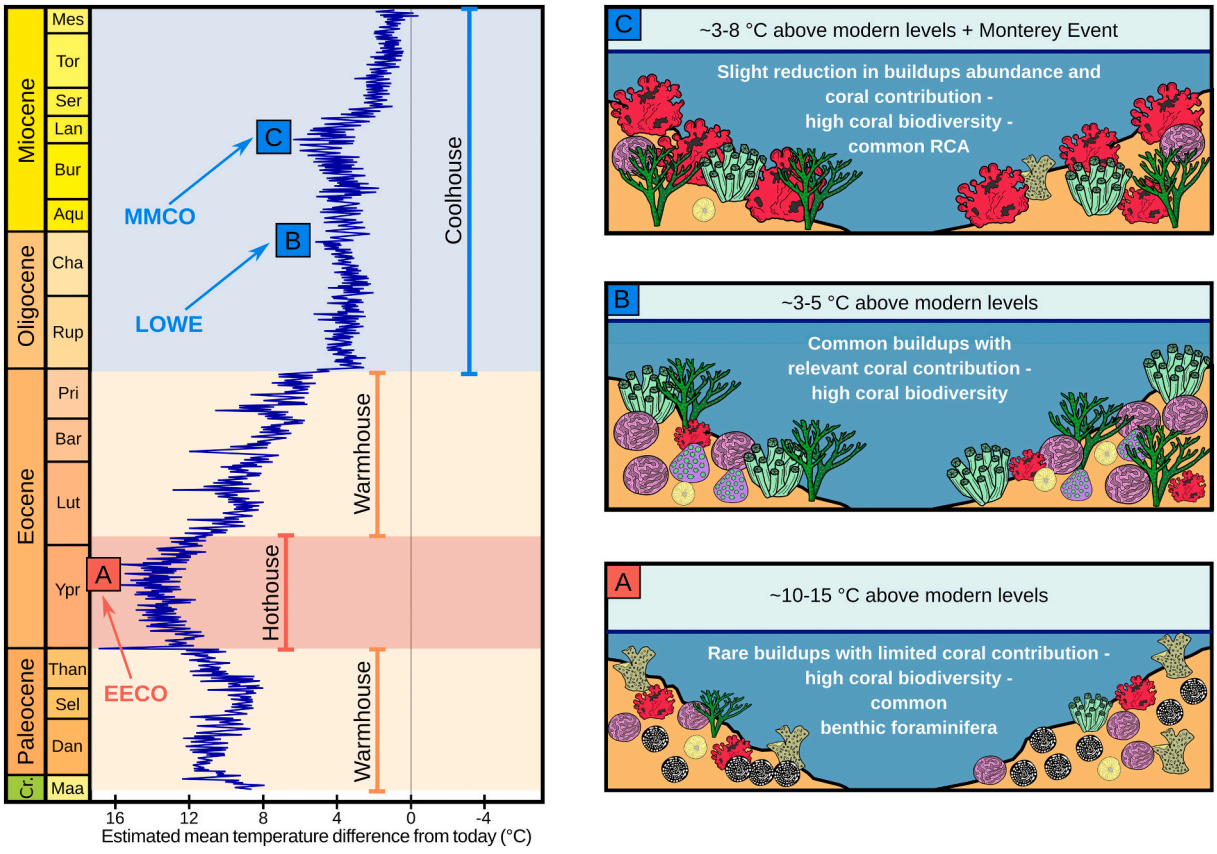

Fig. 6. Coral reef characteristics during the investigated warm intervals of the Cenozoic. On the left, climate states of the Cenozoic and averaged temperature difference from today based on Westerhold et al., 2020. On the right, characteristics of coral reefs during the investigated periods; A) MMCO; B) LOWE; C) EECO.

(Budd, 2000; Bosellini and Perrin, 2012). Our own data indicate a decline in coral carbonate production compared to the upper Oligocene (corals represent approximately 1/3 to 1/2 of the DCP organic buildup, compared to 2/3 in the CL), likely related to increased nutrient availability (Tables 2, 3; Figs. 3, 6).

No coral crisis is recorded during the LOWE. Our results clearly underline that in the upper Oligocene limestones of CL, corals are significantly more abundant than in the other sites (Table 3; Figs. 3, 6). Although in MP and DCP corals also represent the dominant skeletal component within the buildups, at CL they are abundant also in the surrounding facies (Fig. 4), indicating that coral growth was not restricted to the framework itself but extended into associated depositional environments including the internal lagoon and the foreslope. This suggests that, during the Oligocene, the coral-dominated carbonate factory, reached its maximum extent compared to the other two investigated time intervals, despite all intervals being represented by framework reefs, characterized by moderate to high coral diversity (Perrin, 2002). When placed in a broader temporal framework, this pattern underscores the Oligocene as a distinctive phase in the Cenozoic evolution of coral reefs. This interval corresponds to a global peak in reef abundance, marked by the extensive development of coral reefs in both the Caribbean and Tethys (Frost, 1981; Budd, 2000; Perrin, 2002; Johnson et al., 2008; Perrin and Bosellini, 2012). Quantitative analysis of coral-dominated facies in Central Asia, clearly places this peak into the upper Oligocene (Coletti et al., 2022). These Oligocene reef systems were predominantly framework reefs and were characterized by moderate to high coral diversity (Perrin, 2002). Moreover, Oligocene systems show a broad spectrum of reef types occurring in various depositional settings, especially in the Mediterranean region. Together with the Chattian fringing reef complex of the Castro Limestone herein analysed, the Mediterranean region records, for example, the Rupelian barrier reef/lagoon system of the Lessini Shelf (NE Italy; Bosellini and Trevisani, 1992; Bosellini et al., 2020), and the various upper Rupelian-Chattian coral assemblages and patch reefs of the Tertiary Piedmont Basin (NW Italy), the latter associated with fan-delta mixed carbonate-siliciclastic settings and turbid-water conditions (Bosellini et al., 2024). All these key-characteristics (i.e., common, widespread, large and predominantly framework reefs characterized by moderate to high coral diversity) are not as well developed in the Eocene and Miocene reefs as they are in those of the Oligocene, at least for the Mediterranean region. Late Miocene reefs were well developed in size but characterized by a very low coral diversity (for a comprehensive review of Mediterranean Oligocene and Miocene reefs, and associated literature, see Perrin and Bosellini, 2012).

The Oligocene thus represents a phase during which corals achieved both high reef-building efficiency, high diversity, and a broad distribution as carbonate producers (Fig. 6). Following the Eocene/Oligocene Transition (EOT) cooling event, driven by the isolation of Antarctica, and the onset of the circum-Antarctic current, global temperatures increased once more during the Oligocene, especially during the Chattian (Zachos et al., 2001; Burke et al., 2018; Westerhold et al., 2020; Judd et al., 2024). This relatively modest temperature increase has been unexpectedly correlated with declining atmospheric CO_2 values (Zhang et al., 2013; O'Brien et al., 2020) and was not connected to major perturbation in carbon cycle (Westerhold et al., 2020). The associated sea-level rise likely flooded vast coastal plains exposed during the Oi1 glacial events, providing plenty of substrate for coral colonization. The Tethys seaway connecting the reef belt of the Mediterranean Tethys with the Indian Ocean was still a wide oceanic basin during the late Oligocene, promoting the exchange of coral larvae crucial to maintain a high diversity. Other favorable conditions for coral reef growth during the Oligocene include seawater chemistry, especially elevated Mg/Ca ratios enhancing aragonite precipitation (Stanley and Hardie, 1998), optimal regional controls such as the presence of several tectonically stable carbonate platforms, and oligothrophic clear-water conditions (Mutti and Hallock, 2003; Bosellini, 2006; Brandano et al., 2009; Gatt and Gluyas, 2012).

5.3. Skeletal components as proxies for interpreting ancient coral reef ecosystems

The current analysis provides new quantitative data regarding a long-standing question: how reef ecosystems have evolved over time under the pressure of a changing climate. Previous studies have primarily focused on qualitative comparisons of reef-bearing carbonate systems, on the frequency and relevance of reefs within the stratigraphic record, or on reef-coral biodiversity. In this study, the issue is approached by initially assessing the similarities of the investigated carbonate systems, then by analyzing the abundance of other components associated with the reef system, and, subsequently, by using these data to reveal the patterns of the corals themselves. Our results are unlike to represent a mere coincidence or an exception as they align with previous analyses indicating a crisis in coral carbonate production during the EECO (likely related to the interval's extremely high temperatures), a mild decline during the MMCO (potentially linked to increased nutrient availability) and a boom in coral carbonate production during the LOWE (possibly driven by a favorable trophic and chemical marine state combined with limited warming and the high availability of suitable substrates) (Fig. 6).

Furthermore, the current quantitative analysis, and the ordination analysis in particular, paves the way for comparisons with modern settings or reef systems from other time intervals. Among heterotrophs, the distribution of serpulids (SERP) is of particular significance (Fig. 5). The analysis of modern biogenic sediments indicates that the abundance of sessile benthic heterotrophs, such as serpulids, is generally negatively correlated with temperature and light availability (Bialik et al., 2023). Consistent with this, the ordination analysis shows the SERP vector oriented opposite to the LBF vector, the latter being established as positively correlated with temperature. Following the clues provided by the distribution of modern carbonate producers (Bialik et al., 2023), the LBF-SERP axis of our ordination plot could be interpreted as reflecting variability related to temperatures and nutrient availability, highlighting a trend from warm oligotrophic conditions (MP) to cooler (global cooling plus northward movement of the Mediterranean), oligotrophic to mesotrophic conditions (DCP).

Comparing our results with a similar analysis of Upper Miocene reef systems reveals a comparable clustering of vectors related to framework builders, in particular corals and encrusting benthic foraminifera (Fig. 5; Coletti et al., 2026). This indicates shared ecological requirements for these two groups of builders, implying that further analyses of their ratios within the organic buildup facies could yield significant paleoecological insights. Similarly to our current analysis, in the Upper Miocene analysis, *Halimeda* consistently clusters with serpulids and bryozoans (Fig. 5; Coletti et al., 2026), further underscoring a preference of this calcareous green alga for environments characterized by moderate nutrient enrichment (unlike corals).

While quantitative microfacies analysis has previously been employed to characterize carbonate systems, its application for comparing analogous environments across both time (as in this study) and space (e.g., Coletti et al., 2026) has remained limited. Nevertheless, current results highlight the remarkable potential for developing paleoenvironmental proxies based on the specific characteristics of skeletal assemblages. Although presently the currently available datasets from shallow-water environments are still too fragmented and scattered to stand alone, they serve as a vital complement to paleoenvironmental data derived from the deep-sea record. The latter provides a faithful and reliable account of global climatic evolution, but it is often sufficiently decoupled from surface conditions to complicate certain interpretations (e.g., the LOWE; O'Brien et al., 2020). Therefore, although shallow-marine records are more site-sensitive, developing large, cross-comparable datasets of shallow-water successions can provide a "second pillar" to support our understanding of both past and future

climates.

6. Conclusions

Coral reefs underwent significant changes during the Cenozoic, including variations in the overall abundance of coral-dominated buildups, diversity and composition of the assemblage, volume of the buildups, and traits of the corals. Based on a quantitative analysis of skeletal and non-skeletal components from comparable shallow-water systems across key Cenozoic warming intervals (Early Eocene Climatic Optimum, Late Oligocene Warming Event, Middle Miocene Climatic Optimum), our results provide new evidence regarding which compositional features of these coral reefs evolved, and which remained constant:

- The investigated facies are dominated by skeletal grains embedded in a matrix of sand-sized comminuted bioclasts, with other textural components being usually less relevant; this textural similarity is even stronger within the organic buildups. Skeletal assemblages are largely dominated by photozoan producers, and the organic buildups is always dominated by corals. The reef factory keeps its overall structural integrity during the investigated warm intervals, defined by the persistence of textural characteristics. This, in turn, suggests that similar functional roles were maintained, pointing to a long-term stability of the inner organization of the coral reef carbonate factory across a wide range of environmental conditions.
- Significant compositional differences exists between the carbonate factories. Benthic foraminifera are a major component in the lower Eocene site, coral-driven carbonate production is higher in the upper Oligocene site, and calcareous red algae and heterotrophs are more prominent in the Middle Miocene site. These data are consistent with the known large-scale stratigraphic distribution of the various carbonate factory types (i.e., benthic foraminifera, corals, and calcareous algae dominated facies), indicating that the observed shifts reflect production trends controlled by the unique environmental drivers of the three investigated warming events. The prolonged and extreme temperatures of the early Eocene caused a crisis in coral carbonate production, while the milder Middle Miocene warming, associated with a significant perturbation of the carbon cycle, caused a slight decline in coral production, compensated by a relative increase in calcareous red algae. Conversely, the late Oligocene warming did not result in a crisis likely due to a unique combination of oceanographic conditions (i.e., mild temperature increase, low nutrient concentrations, favorable seawater Mg/Ca ratio, and the availability of substrates for colonization) that instead enhanced coral development.
- These dynamics highlight the resilience and adaptability of the coral reef carbonate factory, which remains capable of producing framework reefs—albeit of varying sizes and volumes—even under sub-optimal conditions. Coral carbonate production appear to be significantly compromised only under extremely high temperatures or when multiple stressors acts in synergy.

CRediT authorship contribution statement

Luca Mariani: Writing – review & editing, Writing – original draft, Visualization, Validation, Supervision, Resources, Methodology, Investigation, Formal analysis, Data curation, Conceptualization. **Giovanni Coletti:** Writing – review & editing, Writing – original draft, Visualization, Validation, Supervision, Resources, Methodology, Investigation, Formal analysis, Data curation, Conceptualization. **Alessandro Vescogni:** Writing – review & editing, Writing – original draft, Visualization, Validation, Supervision, Resources, Methodology, Conceptualization. **Alberto Vimercati:** Methodology, Formal analysis, Data curation. **Francesca R. Bosellini:** Writing – review & editing, Writing – original draft, Visualization, Validation, Supervision, Resources, Methodology, Funding acquisition, Conceptualization.

Declaration of Generative AI and AI-assisted technologies in the writing process

During the preparation of this work the authors used Gemini (Google/Alphabet) in order to support the refinement of the language, clarity of expression, and adherence to journal formatting guidelines with regards to the abstract and highlights. The tools were used on an original test to refine its structure. After using the tools, the authors reviewed and edited the content as needed and take full responsibility for the content of the publication.

Declaration of competing interest

The authors declare that they have no known competing financial interests or personal relationships that could have appeared to influence the work reported in this paper.

Acknowledgments

We acknowledge financial support by the European Union – Next Generation EU PRIN MUR 2022WEZE44 to C. Bottini "Conservation of life on Earth: the fossil record as an unparalleled archive of ecological and evolutionary responses to past warming events". We thank the Editor (Dr. Michal Gradzinski), the Guest Editor (Dr. Laura Tomassetti) and two anonymous reviewers for their constructive remarks.

Appendix A. Supplementary data

Supplementary data to this article can be found online at https://doi.org/10.1016/j.sedgeo.2026.107124.

Data availability

All data are included in the main text and in the supplementary material

References

Agnini, C., Fornaciari, E., Raffi, I., Catanzariti, R., Pälike, H., Backman, J., Rio, D., 2014. Biozonation and biochronology of Paleogene calcareous nannofossils from low and middle latitudes. Newsletters on Stratigraphy 47 (2), 131–181.

Aguilera, O., Bencomo, K., de Araújo, O.M.O., Dias, B.B., Coletti, G., Lima, D., Silane A.F. da Silva-Caminha, S.A.F., Polck, M., Alves Martins, M.V., Jaramillo, C., Tavares Kutter, V., Lopes, R.T., 2020. Miocene heterozoan carbonate systems from the western Atlantic equatorial margin in South America: the Pirabas Formation. Sedimentary Geology 407, 105739.

Aguirre, J., Riding, R., Braga, J.C., 2000. Diversity of coralline red algae: origination and extinction patterns from the Early Cretaceous to the Pleistocene. Paleobiology 26 (4), 651–667.

Ali, M., Coletti, G., Garzanti, E., Adatte, T., Castelltort, S., Sternai, P., Benedetti, A., Malinverno, E., Mariani, L., Spangenberg, J.E., Khan, S., Basso, D., Samankassou, E., Kocsis, L., Usman, M., 2025. The Baroch Nala section (NE Pakistan): A new PETM standard for the eastern Tethys. Marine and Petroleum Geology 171, 107183.

Bassant, P., Gürbüz, K., 2005. Guide to the Turkey Carbonates Field Seminar, Mut Basin, 18th/24th September 2005.

Bassant, P., van Buchem, F.S.P., Görür, N., 2005. The stratigraphic architecture and evolution of the Burdigalian carbonate–siliciclastic sedimentary systems of the Mut Basin, Turkey. Sedimentary Geology 173, 187–232.

Bassi, D., Bianchini, G., Mietto, P., Nebelsick, J.H., 2008. Southern Alps in Italy: Venetian Pre-Alps. In: McCann, T. (Ed.), The Geology of Central Europe, v. 2. The Geological Society of London, London, pp. 1087–1092.

Beavington-Penney, S.J., Racey, A., 2004. Ecology of extant nummulitids and other larger benthic foraminifera: applications in palaeoenvironmental analysis. Earth-Science Reviews 67 (3–4), 219–265.

Benedetti, A., Papazzoni, C.A., 2022. Rise and fall of rotaliid foraminifera across the Paleocene and Eocene times. Micropaleontology 68 (2), 185–196.

Benedetti, A., Papazzoni, C.A., Bosellini, F.R., 2024. Unparallel resilience of shallow-water tropical calcifiers (foraminifera and scleractinian reef corals) during the early Paleogene global warming intervals. Palaeogeography, Palaeoclimatology, Palaeoecology 651, 112393.

Bialik, O.M., Jarochowska, E., Grossowicz, M., 2021. Ordination analysis in sedimentology, geochemistry and palaeoenvironment—Background, current trends and recommendations. Depositional Record 7 (3), 541–563.
Bialik, O.M., Coletti, G., Mariani, L., Commissario, L., Desbiolles, F., Meroni, A.N., 2023. Availability and type of energy regulate the global distribution of neritic carbonates. Scientific Reports 13, 19687.
Bosellini, A., 1989. Dynamics of Tethyan carbonate platforms. In: Crevello, P.D., Wilson, J.L., Sarg, J.F., Read, J.F. (Eds.), Controls on carbonate platform and basin platform, 44, pp. 3–13. S.E.P.M. Spec. Publ.
Bosellini, A., Carraro, F., Corsi, M., De Vecchi, G.P., Gatto, G.O., Malaroda, R., Sturani, C., Ungaro, S., Zanettin, B., 1967. Note illustrative della carta geologica d'Italia scala 1: 100.000, foglio 49 Verona. Servizio Geologico d'Italia, Nuova Tecnica Grafica, Roma.
Bosellini, A., Bosellini, F.R., Colalongo, M.L., Parente, M., Russo, A., Vescogni, A., 1999. Stratigraphic architecture of the Salento coast from Capo d'Otranto to S. Maria di Leuca (Apulia, southern Italy). Riv. It. Paleont. Strat. 105, 397–416.
Bosellini, F., Trevisani, E., 1992. Coral facies and cyclicity in the Castelgomberto Limestone (Early Oligocene, Eastern Lessini Mountains, Northern Italy). Rivista Italiana di Paleontologia e Stratigrafia 98, 339–352.
Bosellini, F.R., 2006. Biotic changes and their control on Oligocene–Miocene reefs: a case study from the Apulia Platform margin (southern Italy). Palaeogeography, Palaeoclimatology, Palaeoecology 241, 393–409.
Bosellini, F.R., Perrin, C., 1994. The coral fauna of Vitigliano: qualitative and quantitative analy-sis in a backreef environment (Castro Limestone, Late Oligocene, Salento Peninsula, south-ern Italy). Boll. Soc. Paleont. It. 33, 171–181.
Bosellini, F.R., Perrin, C., 2008. Estimating Mediterranean Oligocene–Miocene sea-surface temperatures: an approach based on coral taxonomic richness. Palaeogeography, Palaeoclimatology, Palaeoecology 258 (1–2), 71–88.
Bosellini, F.R., Perrin, C., 2012. Coral Diversity and Temperature: a Palaeoclimatic Perspective for the Oligo-Miocene of the Mediterranean Region. In: Carbonate Systems during the Oligocene–Miocene Climatic Transition, pp. 229–244.
Bosellini, F.R., Russo, A., 1992. Stratigraphy and facies of an Oligocene fringing reef (Castro Limestone, Salento Peninsula, southern Italy). Facies 26, 146–166.
Bosellini, F.R., Vescogni, A., Kiessling, W., Zoboli, A., Di Giuseppe, D., Papazzoni, C.A., 2020. Revisiting reef models in the Oligocene of northern Italy (Venetian Southern Alps). Bollettino della Societa Paleontologica Italiana 59 (3), 337–348.
Bosellini, F.R., Vescogni, A., Budd, A., Papazzoni, C.A., 2021. High coral diversity is coupled with reef-building capacity during the late Oligocene warming (Castro Limestone, Salento Peninsula, S Italy). Riv. It. Paleont. Strat. 127 (3), 515–538.
Bosellini, F.R., Benedetti, A., Budd, A.F., Papazzoni, C.A., 2022. A coral hotspot from a hot past: The EECO and post-EECO rich reef coralfauna from Friuli (Eocene, NE Italy). Palaeogeography, Palaeoclimatology, Palaeoecology 607, 111284. https://doi.org/10.1016/j.palaeo.2022.111284.
Bosellini, F.R., Vescogni, A., Briguglio, A., Piazza, M., Papazzoni, C.A., Silvestri, G., Morsilli, M., 2024. Resilient coral reef ecosystems: The case study of turbid-mesophotic coral buildups during the Late Oligocene Warming Event (Tertiary Piedmont Basin, NW Italy). Palaeogeography, Palaeoclimatology, Palaeoecology 649, 112330.
Bosellini, F.R., Benedetti, A., Kiessling, W., 2025. Minor coral diversity loss but long-lasting coral reef crises in the early Paleogene hothouse. Paleoceanography and Paleoclimatology 40, e2024PA004985.
Bosellini, F.R., Mariani, L., Benedetti, A., 2026. Trajectories of reef coral morphological traits during the early Paleogene hothouse reveal the predictive limits of fossil analogues in a rapidly changing climate. Palaeogeography, Palaeoclimatology, Palaeoecology 683, 113472. https://doi.org/10.1016/j.palaeo.2025.113472.
Brandano, M., Frezza, V., Tomassetti, L., Pedley, M., Matteucci, R., 2009. Facies analysis and palaeoenvironmental interpretation of the late Oligocene Attard Member (lower Coralline Limestone Formation), Malta. Sedimentology 56 (4), 1138–1158.
Brandano, M., Cornacchia, I., Raffi, I., Tomassetti, L., Agostini, S., 2017. The Monterey Event within the Central Mediterranean area: The shallow-water record. Sedimentology 64 (1), 286–310.
Brandano, M., Tomassetti, L., Mateu-Vicens, G., Gaglianone, G., 2019. The seagrass skeletal assemblage from modern to fossil and from tropical to temperate. Insight from Maldivian and Mediterranean examples. Sedimentology 66 (6), 2268–2296.
Bray, J.R., Curtis, J.T., 1957. An ordination of the upland forest communities of Southern Wisconsin. Ecological Monographs 27 (4), 325–349.
Bridge, T.C.L., Baird, A.H., Pandolfi, J.M., McWilliam, M.J., Zapalski, M.K., 2022. Functional consequences of Palaeozoic reef collapse. Scientific Reports 12, 1386. https://doi.org/10.1038/s41598-022-05154-6.
Budd, A.F., 2000. Diversity and extinction in the Cenozoic history of Caribbean reefs. Coral Reefs 19 (1), 25–35.
Burke, K.D., Williams, J.W., Chandler, M.A., Haywood, A.M., Lunt, D.J., Otto-Bliesner, B. L., 2018. Pliocene and Eocene provide best analogs for near-future climates. Proceedings of the National Academy of Sciences 115 (52), 13288–13293.
Cahuzac, B., Poignant, A., 1997. Essai de biozonation de l'Oligo-Miocène dans les bassins européens à l'aide des grands foraminifères néritiques. Bull. Soc. Géol. Fr. 168, 155–169.
Carminati, E., Lustrino, M., Doglioni, C., 2012. Geodynamic evolution of the central and western Mediterranean: tectonic vs. igneous petrology constraints. Tectonophysic 579, 173–192.
Carpenter, K.E., Abrar, M., Aeby, G., Aronson, R.B., Banks, S., Bruckner, A., et al., 2008. One-Third of Reef-Building Corals Face Elevated Extinction Risk from Climate Change and Local Impacts. Science 321, 560–563. https://doi.org/10.1126/science.1159196.
Carraro, F., Malaroda, R., Piccoli, G., Sturani, C., Venzo, S., 1969. Note Illustrative della Carta Geologica D'Italia, Scala 1:100.000. Foglio 48, Peschiera del Garda. Poligrafica & Cartevalori Ercolano. Napoli.
Cheung, M.W.M., Hock, K., Skirving, W., Mumby, P.J., 2021. Cumulative bleaching undermines systemic resilience of the Great Barrier Reef. Curr. Biol. 31 (23), 5385–5392. https://doi.org/10.1016/j.cub.2021.09.078. ISSN 0960-9822.
Coletti, G., Mariani, L., Garzanti, E., Consani, S., Bosio, G., Vezzoli, G., Hu, X., Basso, D., 2021. Skeletal assemblages and terrigenous input in the Eocene carbonate systems of the Nummulitic Limestone (NW Europe). Sedimentary Geology 425, 106005.
Coletti, G., Commissario, L., Mariani, L., Bosio, G., Desbiolles, F., Soldi, M., Bialik, O.M., 2022. Palaeocene to Miocene southern Tethyan carbonate factories: a meta-analysis of the successions of south-western and western Central Asia. Depositional Record 8 (3), 1031–1054.
Coletti, G., Commissario, L., Ali, M., Mariani, L., Granier, B., Brandano, M., Mancini, A., Rusciadelli, G., Ricci, C., Baceta, J.I., Vicens, G.M., Basso, D., 2025. Coral carbonate production during the Paleocene: insights from the Maiella Massif (Pennapiedimonte, Central Italy). Rivista Italiana di Paleontologia e Stratigrafia 131 (1), 177–200.
Coletti, G., Vimercati, A., Bosellini, F.R., Mariani, L., Guido, A., Vescogni, A., Reolid, J., Auer, G., Basso, D., Collareta, A., Bosio, G., Bialik, O.M., 2026. Quantitative analysis of Upper Miocene Mediterranean reef carbonates: a tool for reconstructing palaeoenvironmental gradients. Palaeogeogr. Palaeoclimatol. Palaeoecol. under review.
Crabbe, M.J.C., 2008. Climate change, global warming and coral reefs: Modelling the effects of temperature. Computational Biology and Chemistry 32 (5), 311–314.
De Zanche, V., Sorbini, L., Spagna, V., 1977. Geologia del territorio del Comune di Verona. Mem. Mus. Civ. Stor. Nat. Verona 1, 1–52.
Dee, S.G., Torres, M.A., Martindale, R.C., Weiss, A., DeLong, K.L., 2019. The Future of Reef Ecosystems in the Gulf of Mexico: Insights from coupled climate Model Simulations and Ancient Hot-House Reefs. Front. Mar. Sci. 6, 691.
Denis, V., Ribas-Deulofeu, L., Sturaro, N., Kuo, C.Y., Chen, C.A., 2017. A functional approach to the structural complexity of coral assemblages based on colony morphological features. Scientific Reports 7 (1), 9849.
Dercourt, J., Gaetani, M., Vrielynk, B., Barrier, E., Biju-Duval, B., Brunet, M.F., Cadet, J. P., Crasquin, S., Sandulescu, M., 2000. Atlas Peri-Tethys, Palaeogeographical maps, p. 279.
Dietzel, A., Bode, M., Connolly, S.R., Hughes, T.P., 2021. The population sizes and global extinction risk of reef-building coral species at biogeographic scales. Nat. Ecol. Evol. 5, 663–669. https://doi.org/10.1038/s41559-021-01441-z.
Dimitrijević, D., Raja, N.B., Kiessling, W., 2023. Corallite sizes of reef corals: decoupling of evolutionary and ecological trends. Paleobiology 50, 43–53. https://doi.org/10.1017/pab.2023.28.
Doglioni, C., Bosellini, A., 1987. Eoalpine and mesoalpine tectonics in the Southern Alps. Geologische Rundschau 77, 734–754.
Eddy, T.D., Lam, V.W.Y., Reygondeau, G., Cisneros-Montemayor, A.M., Greer, K., Palomares, L.M.D., Bruno, J.F., Ota, Y., Cheung, W.W.L., 2021. Global decline in capacity of coral reefs to provide ecosystem services. One Earth 4 (9), 1278–1285. https://doi.org/10.1016/j.oneear.2021.08.016.
Esteban, M., 1996. An overview of Miocene reefs from Mediterranean areas: general trends and facies models.
Flügel, E., 2010. Microfacies of carbonate rocks: analysis, interpretation and application. Springer, Berlin.
Föllmi, K.B., Badertscher, C., de Kaenel, E., Stille, P., John, C.M., Adatte, T., Steinmann, P., 2005. Phosphogenesis and organic-carbon preservation in the Miocene Monterey Formation at Naples Beach, California—The Monterey hypothesis revisited. Geological Society of America Bulletin 117 (5–6), 589–619.
Fontoura, L., Zawada, K.J., D'Agata, S., Alvarez-Noriega, M., Baird, A.H., Boutros, N., Dornelas, M., Luiz, O.J., Madin, J.S., Maina, J.M., 2020. Climate-driven shift in coral morphological structure predicts decline of juvenile reef fishes. Global Change Biology 26, 557–567.
Frost, S.H., 1981. Oligocene reef coral biofacies of the Vicentin, northeast Italy.
Gatt, P.A., Gluyas, P.A., 2012. Climatic controls on facies in Palaeogene Mediterranean subtropical carbonate platforms. Petroleum Geoscience 18, 355–367.
Gauch, H.G., Whittaker, R.H., 1972. Comparison of ordination techniques. Ecology 53 (5), 868–875.
Goldner, A., Herold, N., Huber, M., 2014. The challenge of simulating the warmth of the mid-Miocene climatic optimum in CESM1. Climate of the Past 10 (2), 523–536.
Granier, B.R., 2024. Reassessment of *Iberopora bodeuri*, a primitive plurilocular calcareous encrusting foraminifer from the "Upper Jurassic"(including Berriasian) carbonate platforms of the northern and central Tethys. Cretaceous Research 155, 105782.
Guido, A., Mastandrea, A., Stefani, M., Russo, F., 2016. Role of autochthonous versus detrital micrite in depositional geometries of Middle Triassic carbonate platform systems. GSA Bulletin 128, 989–999.
Guido, A., Palladino, G., Sposato, M., Russo, F., Prosser, G., Bentivenga, M., Mastandrea, A., 2021. Reconstruction of tectonically disrupted carbonates through quantitative microfacies analyses: an example from the Middle Triassic of Southern Italy. Facies 67, 22.
Halfar, J., Mutti, M., 2005. Global dominance of coralline red-algal facies: A response to Miocene oceanographic events. Geology 33, 481–484.
Halfar, J., Godinez-Orta, L., Mutti, M., Valdez-Holguin, J.E., Borges, J.M., 2006. Carbonates calibrated against oceanographic parameters along a latitudinal transect in the Gulf of California. Mexico. Sedimentology 53 (2), 297–320.
Handy, M.R., Ustaszewski, K., Kissling, E., 2015. Reconstructing the Alps-Carpathians-Dinarides as a key to understanding switches in subduction polarity, slab gaps and surface motion. International Journal of Earth Sciences 104, 1–26.

Hill, M.O., 1979. Decorana—A Fortran program for detrended correspondence analysis and reciprocal averaging. Cornell Univ, Section of Ecology and Systematics.
Hoegh-Guldberg, O., Mumby, P.J., Hooten, A.J., Steneck, R.S., Greenfield, P., Gomez, E., Harvell, C.D., Sale, P.F., Edwards, A.J., Caldeira, K., Knowlton, N., Eakin, C.M., Prieto-Iglesias, R., Muthiga, N., Bradbury, R.H., Dubi, A., Hatziolos, M.E., 2007. Coral Reefs under Rapid Climate Change and Ocean Acidification. Science 318 (5857), 1737–1742. https://doi.org/10.1126/science.1152509.
Hottinger, L., 1982. Larger foraminifera, giant cells with a historical background. Naturwissenschaften 69 (8), 361–371.
Hughes, T.P., Barnes, M.L., Bellwood, D.R., Cinner, J.E., Cumming, G.S., Jackson, J.B.C., Kleypas, J., van de Leemput, I.A., Lough, J.M., Morrison, T.H., Palumbi, S.R., van Nes, E.H., Scheffer, M., 2017a. Coral reefs in the Anthropocene. Nature 546, 82–90. https://doi.org/10.1038/nature22901.
Hughes, T.P., Kerry, J.T., Álvarez-Noriega, M., Álvarez-Romero, J.G., Anderson, K.D., Baird, A.H., et al., 2017b. Global warming and recurrent mass bleaching of corals. Nature 543, 373–377. https://doi.org/10.1038/nature21707.
Ilgar, A., Esirtgen, T., Hakyemez, A., Culha, G., Demirkaya, S., Türkmen Bozkurt, B., 2019. The control of sea-level changes on sedimentation in the Mut Basin: late Serravallian-early Tortonian incised valley-fill. Bull. Min. Res. Expl. 159, 1–27.
Inglis, G.N., Bragg, F., Burls, N.J., Cramwinckel, M.J., Evans, D., Foster, G.L., Huber, M., Lunt, D.J., Siler, N., Steinig, S., Tierney, J.E., Wilkinson, R., Anagnostou, E., de Boer, A.M., Dunkley Jones, T., Edgar, K., Hollis, C.J., Hutchinson, D.K., Pancost, R. D., 2020. Global mean surface temperature and climate sensitivity of the early Eocene Climatic Optimum (EECO), Paleocene–Eocene Thermal Maximum (PETM), and latest Paleocene. Climate of the Past 16 (5), 1953–1968. https://doi.org/10.5194/cp-16-1953-2020.
IPCC, 2022. Climate Change 2022: Impacts, Adaptation, and Vulnerability. Cambridge University Press. https://doi.org/10.1017/9781009325844.
Janson, X., Van Buchem, F.S.P., Dromart, G., Eichenseer, H.T., Dellamonica, X., Boichard, R., Bonnaffe, F., Eberli, G., 2010. Architecture and facies differentiation within a Middle Miocene carbonate platform, Emenek, Mut Basin, southern Turkey. Special Publication. Geological Society of London 329, 265–290.
Johnson, K.G., Jackson, J.B., Budd, A.F., 2008. Caribbean reef development was independent of coral diversity over 28 million years. Science 319 (5869), 1521–1523.
Judd, E.J., Tierney, J.E., Lunt, D.J., Montañez, I.P., Huber, B.T., Wing, S.L., Valdes, P.J., 2024. A 485-million-year history of Earth's surface temperature. Science 385 (6715), eadk3705.
Kiessling, W., 2005. Long-term relationships between marine diversity and reef-building. In: Biological Management of Marine Ecosystems. CRC Press, pp. 11–29.
Kiessling, W., Baron-Szabo, R.C., 2004. Extinction and recovery patterns of scleractinian corals at the Cretaceous–Paleogene boundary. Palaeogeography, Palaeoclimatology, Palaeoecology 214 (3), 195–223.
Kiessling, W., Flügel, E., Golonka, J., 1999. Paleoreef maps: evaluation of a comprehensive database on Phanerozoic reefs. AAPG Bulletin 83, 1552–1587.
Kruskal, J.B., 1964. Nonmetric multidimensional scaling: a numerical method. Psychometrika 29, 115–129.
Ladd, H.S., Tracey Jr., J.I., Wells, J.W., Emery, K.O., 1950. Organic growth and sedimentation on an atoll. The Journal of Geology 58 (4), 410–425.
López-Pérez, R.A., 2005. The Cenozoic hermatypic corals in the eastern Pacific: history of research. Earth-Science Reviews 72 (1–2), 67–87.
Luciani, V., 1989. Stratigrafia sequenziale del Terziario nella Catena del Monte Baldo (provincie di Verona e Trento). Memorie di Scienze Geologica 41, 263–351.
Madin, J.S., Hoogenboom, M.O., Connolly, S.R., Darling, E.S., Falster, D.S., Huang, D., Keith, S.A., Mizerek, T., Pandolfi, J.M., Putnam, H.M., Baird, A.H., 2016. A trait-based approach to advance coral reef science. Trends in Ecology & Evolution 31, 419–428. https://doi.org/10.1016/j.tree.2016.02.012.
Madin, J.S., Anderson, K.D., Andreasen, M.H., Bridge, T.C.L., Cairns, S.D., Connolly, S.R., Darling, E.S., Diaz, M., Falster, D.S., Franklin, E.C., Gates, R.D., Harmer, A.M.T., Hoogenboom, M.O., Huang, D., Keith, S.A., Kosnik, M.A., Kuo, C.-Y., Lough, J.M., Lovelock, C.E., Luiz, O., Martinelli, J., Mizerek, T., Pandolfi, J.M., Pochon, X., Pratchett, M.S., Putnam, H.M., Roberts, T.E., Stat, M., Wallace, C.C., Widman, E., Baird, A.H., 2016. The Coral Trait Database, a curated database of trait information for coral species from the global oceans. Scientific Data 3, 160017. https://doi.org/10.1038/sdata.2016.17.
Mariani, L., Coletti, G., Bosio, G., Vicens, G.M., Ali, M., Cavallo, A., Mittempergher, S., Malinverno, E., 2024. Tectonically-controlled biofacies distribution in the Eocene Foraminiferal Limestone (Pag, Croatia): A quantitative-based palaeontological analysis. Sedimentary Geology 472, 106743.
Mariani, L., Coletti, G., Ali, M., Iqbal, M., Shumail, M., Raza Hassan, H.A., Bosellini, F.R., 2025. Quantitative Biofacies Analysis of Upper Oligocene Reef-Coral Neritic Carbonates (Southern Pakistan). Geosciences 15 (4), 129.
Marshall, A.T., Clode, P., 2004. Calcification rate and the effect of temperature in a zooxanthellate and an azooxanthellate scleractinian reef coral. Coral Reefs 23 (2), 218–224.
Márton, E., Zampieri, D., Kázmér, M., Dunkl, I., Frisch, W., 2011. New Paleocene–Eocene paleomagnetic results from the foreland of the Southern Alps confirm decoupling of stable Adria from the African plate. Tectonophysics 504, 89–99.
Mattern, F., 2022. A Compiled Synoptic Table of the Standard Microfacies and Facies Zone System of Flügel (2010): A Practical Tool. SQU Journal for Science 27 (1), 74–76.
Michel, J., Vicens, G.M., Westphal, H., 2011. Modern heterozoan carbonates from a eutrophic tropical shelf (Mauritania). Journal of Sedimentary Research 81 (9), 641–655.
Mihaljević, M., Korpanty, C., Renema, W., Welsh, K., Pandolfi, J.M., 2017. Identifying patterns and drivers of coral diversity in the Central Indo-Pacific marine biodiversity hotspot. Paleobiology 43 (3), 343–364.
Milli, S., Tancredi, S., Margiotta, S., Tentori, D., 2024. The orogenic effects on forebulge evolution: A case study from Cenozoic deposits in the Salento Peninsula. Italy. Mar. Petrol. Geol. 161, 106698.
Muscio, G., Tintori, A., 2005. I fossili di Bolca – tesori dalle rocce. Catalogo della mostra di Venezia. Museo di Storia Naturale, Venezia.
Mutti, M., Hallock, P., 2003. Carbonate systems along nutrient and temperature gradients: some sedimentological and geochemical constraints. International Journal of Earth Sciences 92, 465–475.
O'Brien, C.L., Huber, M., Thomas, E., Pagani, M., Super, J.R., Elder, L.E., Hull, P.M., 2020. The enigma of Oligocene climate and global surface temperature evolution. Proceedings of the National Academy of Sciences 117 (41), 25302–25309.
Pandolfi, J.M., Kiessling, W., 2014. Gaining insights from past reefs to inform understanding of coral reef response to global climate change. COSUST 7, 52–58.
Pandolfi, J.M., Bradbury, R.H., Sala, E., Hughes, T.P., Bjorndal, K.A., Cooke, R.G., McArdle, D., McClenachan, L., Newman, M.J., Paredes, G., Warner, R.R., Jackson, J. B., 2003. Global trajectories of the long-term decline of coral reef ecosystems. Science 301, 955–958.
Parente, M., 1994. A revised stratigraphy of the Upper Cretaceous to Oligocene units from southeastern Salento (Apulia, southern Italy). Boll. Soc. Paleont. It. 33, 155–170.
Perrin, C., 2002. Tertiary: the emergence of modern reef ecosystems.
Perrin, C., Bosellini, F.R., 2012. Paleobiogeography of scleractinian reef corals: changing patterns during the Oligocene–Miocene climatic transition in the Mediterranean. Earth-Science Reviews 111 (1–2), 1–24.
Perrin, C., Bosellini, F.R., 2013. The Late Miocene coldspot of z-coral diversity in the Mediterranean: Patterns and causes. Comptes Rendus Palevol 12 (5), 245–255. https://doi.org/10.1016/j.crpv.2013.05.010.
Perrin, C., Kiessling, W., 2012. Latitudinal trends in Cenozoic reef patterns and their relationship to climate. Carbonate systems during the Oligocene–Miocene climatic transition 17–33.
Plaziat, J.C., Perrin, C., 1992. Multikilometer-sized reefs built by foraminifera (*Solenomeris*) from the early Eocene of the Pyrenean domain (S. France, N. Spain): Palaeoecologic relations with coral reefs. Palaeogeography, Palaeoclimatology, Palaeoecology 96 (3–4), 195–231.
Pomar, L., 2001. Types of carbonate platforms: a genetic approach. Earth-Science Reviews 54 (4), 313–337.
Pomar, L., Hallock, P., 2008. Carbonate factories: A conundrum in sedimentary geology. Earth-Science Reviews 87 (1–2), 32–69.
Pomar, L., Mateu-Vicens, G., Morsilli, M., Brandano, M., 2014. Carbonate ramp evolution during the Late Oligocene (Chattian), Salento Peninsula, southern Italy. Palaeogeography Palaeoclimatology Palaeoecology 404, 109–132.
Pomar, L., Baceta, J.I., Hallock, P., Mateu-Vicens, G., Basso, D., 2017. Reef building and carbonate production modes in the west-central Tethys during the Cenozoic. Marine and Petroleum Geology 83, 261–304.
Pyko, I., Wisshak, M., Teichert, S., 2025. Depth-related controls on the quantitative composition of rhodolith matrices in the High Arctic. Aquatic Conservation: Marine and Freshwater Ecosystems 35 (1), e70045.
Rae, J.W., Zhang, Y.G., Liu, X., Foster, G.L., Stoll, H.M., Whiteford, R.D., 2021. Atmospheric CO_2 over the past 66 million years from marine archives. Annual Review of Earth and Planetary Sciences 49 (1), 609–641.
Raja, N.B., Dimitrijević, D., Krause, M.C., Kiessling, W., 2022. Ancient Reef Traits, a database of trait information for reef-building organisms over the Phanerozoic. Scientific Data 9, 425. https://doi.org/10.1038/s41597-022-01486-0.
Rankey, E.C., Garza-Pérez, J.R., 2012. Seascape metrics of shelf-margin reefs and reef sand aprons of Holocene carbonate platforms. Journal of Sedimentary Research 82 (1), 53–71.
Reijmer, J.J.G., 2021. Marine carbonate factories: Review and update. Sedimentology 68, 1729–1796.
Reolid, J., Bialik, O.M., Lindhorst, S., Eisermann, J.O., Petrovic, A., Hincke, C., Betzler, C., 2024. A new type of *Halimeda* bioherm on the Queensland Plateau, NE Australia. Coral Reefs 43 (4), 801.
Ricchetti, G., Ciaranfi, N., 2013. Note illustrative della Carta Geologica d'Italia alla scala 1:50.000 – foglio 537 Capo Santa Maria di Leuca. ISPRA – Servizio Geologico d'Italia, Litografia Artistica Cartografica, Firenze, p. 121.
Rossi, D., 1969. Foglio 215. Otranto. Note Illustrative Carta Geologica Italia. Servizio Geologico Italiano, p. 31.
Sarkar, S., Ghosh, A.K., 2013. Coral bleaching a nemesis for the Andaman reefs: Building an improved conservation paradigm. Ocean and Coastal Management 71, 153–162.
Sarkar, S., Cotton, L.J., Valdes, P.J., Schmidt., D.N., 2022. Shallow water records of the PETM: novel insights from NE India (eastern Tethys). Paleoceanography and Paleoclimatology 37, e2021PA004257.
Sarti, M., 1980. Frane sottomarine e debris flow in una successione carbonatico torbiditica eocenica (Val d'Avesa, Verona). Ann. Univ. Ferrara Sez. IX Sci. Geol. Paleont. 7, 65–89.
Scheibner, C., Speijer, R.P., 2008. Late Paleocene–early Eocene Tethyan carbonate platform evolution—a response to long-and short-term paleoclimatic change. Earth-Science Reviews 90 (3–4), 71–102.
Schmid, S.M., Fügenschuh, B., Kissling, E., Schuster, R., 2004. Tectonic map and overall architecture of the Alpine orogen. Eclogae Geologicae Helvetiae 97, 93–117.
Scotese, C.R., Song, H., Mills, B.J., van der Meer, D.G., 2021. Phanerozoic paleotemperatures: The earth's changing climate during the last 540 million years. Earth-Science Reviews 215, 103503.

Serra-Kiel, J., Hottinger, L., Caus, E., Drobne, K., Ferràndez, C., Jauhri, A.K., Less, G., Pavlovec, R., Pignatti, J., Samsó, J.M., Schaub, H., Sirel, E., Strougo, A., Tambareau, Y., Tosquella, J., Zakrevskaya, E., 1998. Larger foraminiferal biostratigraphy of the Tethyan Paleocene and Eocene. Bull. Soc. Géol. Fr 169, 281–299.

Stanley, S.M., Hardie, L.A., 1998. Secular oscillations in the carbonate mineralogy of reef-building and sediment-producing organisms driven by tectonically forced shifts in seawater chemistry. Palaeogeography, Palaeoclimatology, Palaeoecology 144, 3–19. ISSN 0031-0182,. https://doi.org/10.1016/S0031-0182(98)00109-6.

Steinthorsdottir, M., Coxall, H.K., De Boer, A.M., Huber, M., Barbolini, N., Bradshaw, C. D., Strömberg, C.A.E., 2021. The Miocene: The future of the past. Paleoceanography and Paleoclimatology 36 (4), e2020PA004037.

Syms, C., 2008. Ordination. In: Jørgensen, S.E., Fath, B.D. (Eds.), Encycl. Ecol. Elsevier, Amsterdam, pp. 2572–2581.

Teichberg, M., Fricke, A., Bischof, K., 2013. Increased physiological performance of the calcifying green macroalga *Halimeda opuntia* in response to experimental nutrient enrichment on a Caribbean coral reef. Aquatic Botany 104, 25–33.

Teichert, S., 2014. Hollow rhodoliths increase Svalbard's shelf biodiversity. Scientific Reports 4 (1), 6972.

Tierney, J.E., Poulsen, C.J., Montañez, I.P., Bhattacharya, T., Feng, R., Ford, H.L., Hönisch, B., Inglis, G.N., Petersen, S.V., Sagoo, N., Tabor, C.R., Thirumalai, K., Zhu, J., Burls, N.J., Foster, G.L., Goddéris, Y., Huber, B.T., Ivany, L.C., Turner, S.K., Lunt, D.J., McElwain, J.C., Mills, B.J.W., Otto-Bliesner, B.L., Ridgwell, A., Zhang, Y. G., 2020. Past climates inform our future. Science 370, eaay3701. https://doi.org/10.1126/science.aay3701.

Titelboim, D., Almogi-Labin, A., Herut, B., Kucera, M., Asckenazi-Polivoda, S., Abramovich, S., 2019. Thermal tolerance and range expansion of invasive foraminifera under climate changes. Scientific Reports 9 (1), 4198.

Ungaro, S., 2001. Le biofacies paleoceniche ed eoceniche dei Monti Lessini (Veneto, Italia). Ann. Univ. Ferrara Sez. Sci. Terra 9, 1–40.

Vescogni, A., Bosellini, F.R., Cipriani, A., Gurler, G., Ilgar, A., Paganelli, E., 2014. The Dağpazarı carbonate platform (Mut Basin, Southern Turkey): facies and environmental reconstruction of a coral reef system during the Middle Miocene Climatic Optimum. Palaeogeography Palaeoclimatology Palaeoecology 410, 213–232.

Vescogni, A., Bosellini, F.R., Papazzoni, C.A., Giusberti, L., Roghi, G., Fornaciari, E., Dominici, G., Zorzin, R., 2016. Coralgal buildups associated with the Bolca Fossil-Lagerstätten: new evidences from the Ypresian of Monte Postale (NE Italy). Facies 62, 21.

Westerhold, T., Marwan, N., Drury, A.J., Liebrand, D., Agnini, C., Anagnostou, E., Barnet, J.S.K., Bohaty, S.M., De Vleeschouwer, D., Florindo, F., Frederichs, T., Hodell, D.A., Holbourn, A.E., Kroon, D., Lauretano, V., Littler, K., Lourens, L.J., Lyle, M., Palike, H., Rohl, U., Tian, J., Wilkens, R.H., Wilson, P.A., Zachos, J.C., 2020. An astronomically dated record of Earth's climate and its predictability over the last 66 million years. Science 369, 1383–1387.

Westphal, H., Halfar, J., Freiwald, A., 2010. Heterozoan carbonates in subtropical to tropical settings in the present and past. International Journal of Earth Sciences 99 (Suppl. 1), 153–169.

Wiedl, T., Harzhauser, M., Kroh, A., Ćorić, S., Piller, W.E., 2013. Ecospace variability along a carbonate platform at the northern boundary of the Miocene reef belt (Upper Langhian, Austria). Palaeogeography, Palaeoclimatology, Palaeoecology 370, 232–246.

Wilson, J.L., 1975. Carbonate Facies in Geologic History. Springer, New York.

You, Y., Huber, M., Müller, R., Poulsen, C.J., Ribbe, J., 2009. Simulation of the middle Miocene climate optimum. Geophysical Research Letters 36 (4).

Zachos, J.C., Pagani, M., Sloan, L., Thomas, E., Billups, K., 2001. Trends, rhythms and aberrations in global climate 65 Ma to present. Science 292, 686–693.

Zamagni, J., Mutti, M., Košir, A., 2012. The evolution of mid Paleocene–early Eocene coral communities: How to survive during rapid global warming. Palaeogeogr., Palaeoclimatol. Palaeoecol 317–318, 48–65. https://doi.org/10.1016/j.palaeo.2011.12.010.

Zhang, Y.G., Pagani, M., Zhonghui, L., Bohaty, S.M., DeConto, R., 2013. A 40-million-year history of atmospheric CO_2. Philosophical Transactions of the Royal Society A 371, 20130096.